Calibration of Iodide-CIMS for oxygenated hydrocarbons in the gas-phase: Application to measure Henry's Law of 1,2-ISOPOOH

by

Joseph Patrick D'Alesio

B.S., Creighton University, 2020

A thesis submitted to the
Faculty of the Graduate School of the
University of Colorado in partial fulfillment
of the requirements for the degree of
Master of Science
Department of Chemistry
2022

Committee Members:
Rainer Volkamer, Chair
Eleanor Browne
Joost de Gouw

D'Alesio, Joseph Patrick (M.S., Chemistry)

Calibration of Iodide-CIMS for oxygenated hydrocarbons in the gas-phase: Application to measure Henry's Law of 1,2-ISOPOOH

Thesis directed by Prof. Rainer Volkamer

Two gas-phase quantification methods for Chemical Ionization Mass Spectrometry using Iodide reagent ions (Iodide-CIMS) were developed in this work: the integration method and the flow rate method. Both methods utilize a Hamilton syringe pump to relate the detected signal to the gas-phase concentration, also known as a calibration coefficient, injected into a VOCUS 2R API-LToF mass spectrometer configured with an AIM source and equipped with VUV light to generate iodide reagent ions. These quantification methods can be combined with any chemical ionization mass spectrometer utilizing a large variety of target analytes. The integration method was used to determine a calibration coefficient, which was applied to partitioning experiments in order to determine the Henry's Law coefficient for 1,2-ISOPOOH. Henry's Law describes the ratio of the presence of a compound in the aqueous-phase and the gas-phase when partitioning is in equilibrium. Henry's Law applies only to dilute solutions. The 1,2-ISOPOOH Henry's Law coefficient was determined to be 2.61E+05 M/atm +/- 1.81E+04 M/atm. The reported value is bracketed by available literature values, which range from 1.00E+05 M/atm to 1.30E+06 M/atm. The flow rate method was used during initial calibration development to determine preliminary calibration coefficients for a suite of atmospherically relevant acids. This method will continue to be optimized for future laboratory and aircraft calibrations.

Dedication

To my brother - I hope that science reaffirms your appreciation for the beauty of nature and the wondrous opportunities for humanity.

Acknowledgements

I want to acknowledge and thank my advisor, Rainer Volkamer, for his support and guidance. Thank you for challenging me at every step of this journey. I am grateful for the opportunity to have been a member of the Volkamer group and collaborate with innovative and passionate individuals. I also want to thank my committee for their support, insight, and contributions to making the chemistry department a place of learning and growing.

I want to thank my family for their unconditional love and support in this lifetime. You have gifted me with a love of learning that I will take forward to every adventure I embark upon. This accomplishment is not mine but ours.

I want to thank each and every member of the Volkamer group for welcoming me with open arms and a willingness to mentor me and learn together. Thank you Andrea, Chris, Henning, Johana, Kyle, Margarita, Prakriti, Randall, and Ted. I want to especially thank Andrea and Randall for the countless hours spent in and out of the lab imparting your knowledge. I also want to thank Benjamin Deming, Jason D. Surratt, Joel A. Thornton, Zhenfa Zhang, and Paul Ziemann for their work, support, and conversations on the salting project.

This material is based upon work funded by the United States Department of Energy Atmospheric Systems Research program (DE-SC0018221) and US National Science Foundation (AGS-2027252).

Table of Contents

List of Figures

List of Tables

1 Introduction

1.1 The Atmospheric Chemistry of Isoprene

A lot of focus is placed on the emissions of monoterpenes; however, Isoprene is the predominant biogenic source of hydrocarbon emitted into the atmosphere from vegetation. This emission is roughly equal to the total global emission of methane [1] and contributes to one-third of global non-methane volatile organic carbon (VOC) emissions. The Model of Emissions of Gases and Aerosols from Nature (MEGAN) estimates the annual global isoprene emission to be around 500 to 750 Tg. Methane and isoprene dominate the global annual VOC flux into the atmosphere [2]. As Rivera Rios points out in his dissertation, VOC reactivity has an impact on the atmospheric oxidative capacity. The atmospheric oxidative capacity (AOC) is dominated by the OH radical and refers to the process in which freshly emitted substances are converted into secondary products. According to Alfonso Saiz-Lopez et al., the oxidizing capacity of the atmosphere is "the capacity of the atmosphere to oxidize and ultimately remove the large variety of organic and inorganic species which are emitted into it from both natural and anthropogenic sources." This process takes place through the catalytic destruction of ozone which in turn changes the important radical species, such as and most importantly OH, which regulates the oxidizing chemistry [3]. The result of the oxidation is the formation of secondary compounds such as ozone and secondary organic aerosol (SOA). Particulate organic matter, known as organic aerosol (OA), makes up a major component of submicron-sized atmospheric aerosol across the globe [4]. SOA makes up around 30-60% of ambient OAs in urban environments and upwards of 70% in rural areas [5]. SOA formation is also predicted to be from gas-phase oxidation of precursor VOCs with low-enough product saturation vapor pressures to

partition into the aerosol phase [6].Particulate matter, such as SOA, has an effect on human health as it can enter the lungs and the bloodstream. SOA also has an effect on radiative forcing, the water cycle, and cloud formation, all of which affect the climate and the environment[1].

In the first step of VOC oxidation, a peroxy radical (RO_2) is formed and reacts with either HO_2 or NO. In a pristine atmospheric environment, the fate of RO_2 is dominated by the reaction pathway with HO_2. Pristine reaction products of isoprene are hydroxy hydroperoxides (ISOPOOHs). ISOPOOHs differ significantly in both chemical and physical properties from their urban (non-pristine) counterparts. One of these differences is in the radical chain propagation properties which directly impacts secondary compound production and oxidative capacity. In order to predict how ISOPOOHs will affect secondary compound concentrations and oxidative capacity, we must be able to have accurate atmospheric models. Rios references modeling work that reports approximately 30% of global isoprene RO_2 reacting with NO (the non-pristine pathway). While the HO_x reaction pathway is already the dominant one in most locations, it's contributions to atmospheric chemistry will only rise as political regulations for NO_x emissions increase.

Isoprene is a precursor for SOA via two different pathways: 1) The partitioning of semivolatile oxidation products into the organic aerosol phase and 2) The dissolution of soluble species into the aqueous aerosol phase (aqSOA). Glyoxal, methylglyoxal, and isoprene epoxydiol (IEPOX) are all ubiquitous water-soluble gas-phase oxidation products of isoprene that can partition into aerosol liquid water (ALW) and clouds, forming aqSOA. With a high saturation vapor pressure and chemical reactivity, glyoxal is an important precursor for SOA [7] and an example of a molecule that "salts-in". As such, glyoxal has drawn attention to the possibility that other molecules may

form aqSOA via the aqueous phase. ISOPOOHs are the main first-generation products of isoprene oxidation under low-NO_x conditions. Because the compounds have two high hydrophilic functional groups, ISOPOOHs are able to partition into atmospheric water. If ISOPOOHs partition more into atmospheric water, it will contribute more to the aqueous SOA growth [1].1,2-ISOPOOH is a precursor for IEPOX. Thus, a motivation for studying the Henry's Law coefficient of 1,2-ISOPOOH is to determine the likelihood for the molecule to partition to cloud water, and possibly also to aerosol water [8]. Because of this, it is imperative to understand the distribution of the phases in the atmosphere [9].

1.2 The Henry's Law Coefficient

The Henry's Law coefficient is the equilibrium at which the amount of dissolved gas in a liquid is proportional to its partial pressure above the liquid, described by the following equation: C_{aq} = H * p_{sat} where C_{aq} is the aqueous concentration in M, H is the Henry's Law coefficient in M/atm, and p_{gas} is the partial pressure of the gas [9]. The presence of inorganic or organic salts changes the partitioning behavior (known as the salting effect) between the gas and the liquid. This salting behavior can be quantitatively described for neutral organic solutes by the Setschenow equation [10] [11]: $\ln(H_{no\ salt}/H_{salt})$ = k_s * c_{salt} where $H_{no\ salt}$ is the Henry's Law coefficient for a solution with no salt, H_{salt} is the Henry's Law coefficient for a solution with salt, k_s is the Setschenow coefficient, and c_{salt} is the concentration of the salt solution [12] [5]. The salting effect is an important consideration as it can have tremendous effect of SOA growth. An increase in solubility of the organic phase (1,2-ISOPOOH in this case) is referred to as "salting in". A decrease in the solubility of the organic phase is referred to as "salting out". This salting effect modifies the partitioning of the species between

gas and aqueous phase. "Salting in" favors partitioning towards the aqueous phase and in turn increases the precursor molecules available to participate in reactions and SOA formation [13]. "Salting out" favors partitioning towards the gas phase and in turn decreases the precursor molecules available to participate in reactions and SOA formation. Considering this, the Henry's Law coefficient is a function of the environmental conditions (temperature, pressure, etc) from which it is measured [6].

1.3 Sources and Effects of Atmospheric Iodine

The ocean surface is responsible for the dominant, global source of inorganic iodine. Emissions of Volatile inorganic iodine species, hypoiodous acid (HOI) and molecular iodine (I_2), are stimulated by ozone (O_3) at a rate of approximately 1.86 Tg/year. Oceans are also responsible for the dominant source of atmospheric organic iodine, methyl iodide (CH_3I) [14]. Through biotic and photochemical processes, CH_3I and other very short-lived (VSL) iodocarbons (CH_2I_2, C_2H_5I, C_3H_7I, CH_2ICl, CH_2IBr) are produced and released into the atmosphere from the supersaturated ocean waters [15]. The natural source of atmospheric iodine that is easiest to quantify is the photolysis of CH_3I: CH_3I + hv -> CH_3 + I. Lovelock et al. [1973] first observed CH_3I in the atmosphere in the parts-per-trillion (ppt) range. The highest levels of CH_3I were measured in industrialized areas. The lowest levels were observed in remote areas with a pristine atmosphere. In regards to the natural troposphere, marine areas had systematically higher CH_3I concentration levels than continental areas [16]. Top-down estimates of annual ocean emissions of CH_3I are reported as 191 Gg/year by Bell et al. and 550 Gg/year by Butler et al. covering seven cruises across the Atlantic, Pacific, and Southern Oceans [3]. Work in 1980 by Chameides and Davis and then again in

1994 by Soloman demonstrate the rapid, tropospheric photo-dissociation of both organic and inorganic iodine compounds in order to release iodine atoms. These iodine ions then go on to primarily react with ozone to generate IO [15]. The 2018 WMO Ozone Assessment first recognized measurements of iodine oxide (IO) radicals in the tropical transition layer during the Tropical Ocean tRoposphere Exchange of Reactive halogen species and Oxygenated VOC (TORERO) project. The CONvective Transport of Active Species in the Tropics (CONTRAST) campaign first quantified IO radicals in the stratosphere using Differential Optical Absorption Spectroscopy (DOAS). I and IO are collectively referred to as reactive iodine (IO_x = I + IO). Reactive iodine and other species combine to generate different forms of inorganic iodine. Because IO has a fast photolysis, a steady state between I and IO is established [15]. Koenig 2020 suggests that reactive iodine species can be transported from the lower troposphere to the upper troposphere-lower stratosphere via convection. This could account for the reported one third of iodine-induced ozone loss within the lower stratosphere [17].

From a biological perspective, iodine is an essential dietary element for mammals. Thus, the transportation of iodine from its oceanic sources to the continents serves an important role. However, the presence of iodine in the atmosphere also has some important consequences [3]. The most well-known atmospheric policy to date, The Montreal Protocol, phased out emissions of ozone-depleting halocarbons with a major emphasis on chlorine containing compounds. The Montreal protocol is widely considered a policy success story that is confirmed by field observations of ozone trends in the upper troposphere. However, recent trends have also indicated a decline in lower stratospheric ozone. The global climate models used by the Montreal Protocol to evaluate stratospheric ozone recovery do not currently consider iodine chemistry. However, Iodine can destroy ozone 400-1000 times more effectively

than chlorine can. As such, small amounts of iodine can significantly modify ozone. Contributing up to 30% of the attributed ozone destruction in the marine boundary layer (MBL) and upper troposphere (UT) through catalytic reaction cycles, iodine is widespread throughout the troposphere. Iodine is responsible for reducing the tropospheric ozone burden by 9%, modifying the oxidative capacity through OH radicals, and lengthening the lifetime of methane [17]. Because atmospheric iodine species exist in low abundance and have short lifetimes, understanding iodine chemistry and iodine-driven new-particle formation requires high time resolution, high sensitivity, and the ability to simultaneously measure several different iodine species. Previous measurements of atmospheric iodine include the detection of more abundant iodine species, such as molecular iodine (I_2), iodine monoxide (IO), and iodine dioxide (OIO) using the following methods: Differential optical absorption (Leigh et al., 2010), Cavity ring-down (Bitter et al., 2005), Cavity-enhanced absorption (Vaughan et al., 2008), Laser-induced fluorescence (Dillon et al.., 2006), and Resonance fluorescence (Gómez Martín et al., 2011). While spectroscopic techniques offer invaluable insights, these instruments are specificity limited and less sensitive to hypoiodous acid (HOI) and iodic acid (HIO_3) [18]. Most atmospheric measurements of reactive iodine species in the MBL have utilized DOAS to several kilometers over coastal locations. An issue with the DOAS technique is its insensitivity to inhomogeneities in the spatial distribution of iodine species over an integrated path length. Biological coastal emissions of iodine precursors are localized and short lived in the atmosphere; thus, it is imperative to detect these inhomogeneities. Mass spectrometry in conjunction with DOAS allows this detection and offers a more quantitative picture of atmospheric species [3].

1.4 TI^{3}GER and Mass Spectrometry to Study Atmospheric Iodine Chemistry

The Technological Innovation Into Iodine for GV Environmental Research (TI^{3}GER) campaign utilized the National Science Foundation (NSF) and the National Center for Atmospheric Research (NCAR) Gulfstream V (GV) research aircraft to further study atmospheric iodine chemistry. The NSF/NCAR Highly Instrumented Airborne Platform for Environmental Research (HIAPER) GV research aircraft supports a suite of instruments with capabilities to advise understudied chemistry of "climate active gases" responsible for ozone modification and new particle formation in the upper troposphere and lower stratosphere (UTLS). A Tofwerk LTOF mass spectrometer combined with the VOCUS AIM ion source and a nitrate ion source is one of the instruments within this novel collection and was operated in bromine, iodine, and nitrate modes throughout the course of the campaign [19]. With a high time-resolution, a low detection limit, and high selectivity, iodide chemical ionization mass spectrometry (CIMS) can be used to quantify highly functionalized, low-volatility compounds and reactive compounds such as VOCs and inorganic radicals. The formation of ion-molecule adducts containing iodide and bromide is an important approach to measure molecular halogens and halogen oxide radicals as the chemical ionization pathway ensures minimum fragmentation during ionization, thus preserving the parent molecule composition [20]. Iodide CIMS is a particularly attractive option for CIMS applications as the iodide adduct formation occurs at the collisional limit, allowing for maximum sensitivity measurements [17]. Furthermore, iodide is electronegative and a weak gas-phase base. Due to this, both electron transfer and proton abstraction are negligible considerations for atmospherically relevant compounds except for nitrate (NO_3) radicals and sulfuric acid (H_2SO_4). Another reason iodide is commonly chosen as a reagent ion is its large mass-to-charge ratio (m/Q = 126.905 Th) and large mass defect (-0.096

Th). These properties provide an extra degree of ion separation during measurements, allowing for greater selectivity and a lower detection limit at exact mass-to-charge ratios [20].

1.5 Contributions to Atmospheric Chemistry Research

The work presented in this thesis focuses on method development for the quantification of gas-phase signals utilizing a Hamilton syringe pump and a Time-of-Flight Chemical Ionization mass spectrometer (TOF-CIMS). The developed gas-phase quantification methods, the integration method and the flow rate method, are applied to determine the Henry's Law coefficient for 1,2-ISOPOOH and to determine preliminary calibration coefficients for a collection of atmospherically relevant molecules during initial calibration testing for the TI^{3}GER campaign.

2 Description of the Methods

2.1 Syringe Pump Hardware Overview

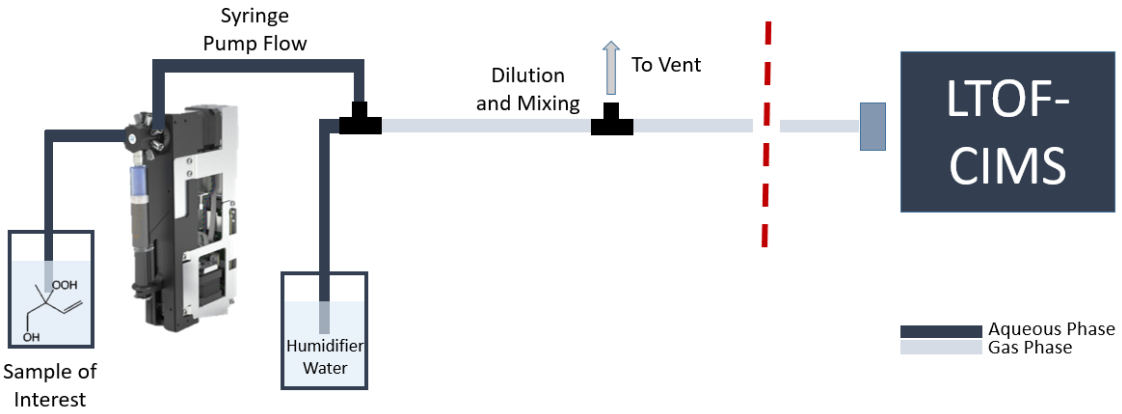

FIGURE 2.1: The figure above displays the Hamilton syringe pump used in both developed gas-phase quantification methods. The syringe pump (left) utilizes a y-valve to aspirate the syringe with the sample of interest (1,2-ISOPOOH in the figure) and then dispense the sample into a t-piece. Water humidified with N_2 gas flows over the sample, which evaporates into the gas-phase. The gas-phase sample is carried into the LTOF-CIMS with overflow exiting at the vent.

The syringe pump setup consists of a 20 mL scintillation vial with a piece of 1/8" OD Teflon tubing bored through the cap. This tubing is connected to the input port of the pump's software-controlled y-valve. The dispensing port of the y-valve is connected to a 250 mL gastight glass syringe. The output port of the valve is fitted to another piece of 1/8" OD Teflon tubing, which is coupled to a Teflon t-piece. When prompted, the syringe pump dispenses a sample droplet from the tip of the Teflon tubing into this t-piece. Humidified N_2 gas is passed over the droplet to fully evaporate the suspended sample droplet. The sample, now in gas form, is transported with the humidified N_2 gas through the Teflon tubing and into the CIMS. Excess flow is vented before entrance into the CIMS. The method, as described above, is a simplification in

order to describe the working parts of the syringe pump setup. This particular syringe pump was chosen for its volume capabilities and for its material that would be in contact with the aqueous samples. The PSD/6 syringe pump has a volume range that spans from microliters to liters. For this particular application, microliter volumes are needed in order to evaporate the samples at a rate that will allow for a quantifiable gas-phase signal measurement. The components of the syringe pump that will be in contact with the samples are made of polytetrafluoroethylene (PTFE), also known as Teflon. Pagonis et al. 2017 and Deming et al. 2019 report that PTFE has the fastest line response time for gas-wall interactions. As such, it is beneficial that the components of the syringe pump that are in contact with the samples be of a PTFE material [21] [22].

2.2 Syringe Pump Software Overview

The user communicates with the syringe pump via a LabView program (Figure 2.2) adapted from Dr. Andrea Wagner's work on a similar instrument that also utilizes a serial communication interface. Programs used to control the Hamilton syringe pumps follow a general flow in which the user initializes the pump, sends commands to the pump, and receives a response from the pump indicating the status of the command. This particular LabView program offers an accessible interface by which the user can initialize the pump, check the pump, syringe, and valve status, and send commands to the pump from the terminal command line. Documentation for the gas-phase quantification methods discussed in this thesis can be found in the appendix.

2.3 Syringe Pump Optimization

Pending the arrival of the LTOF-CIMS, the syringe pump was setup and optimized with a quadrupole CIMS (quad-CIMS) instrument. During this time, the setup was

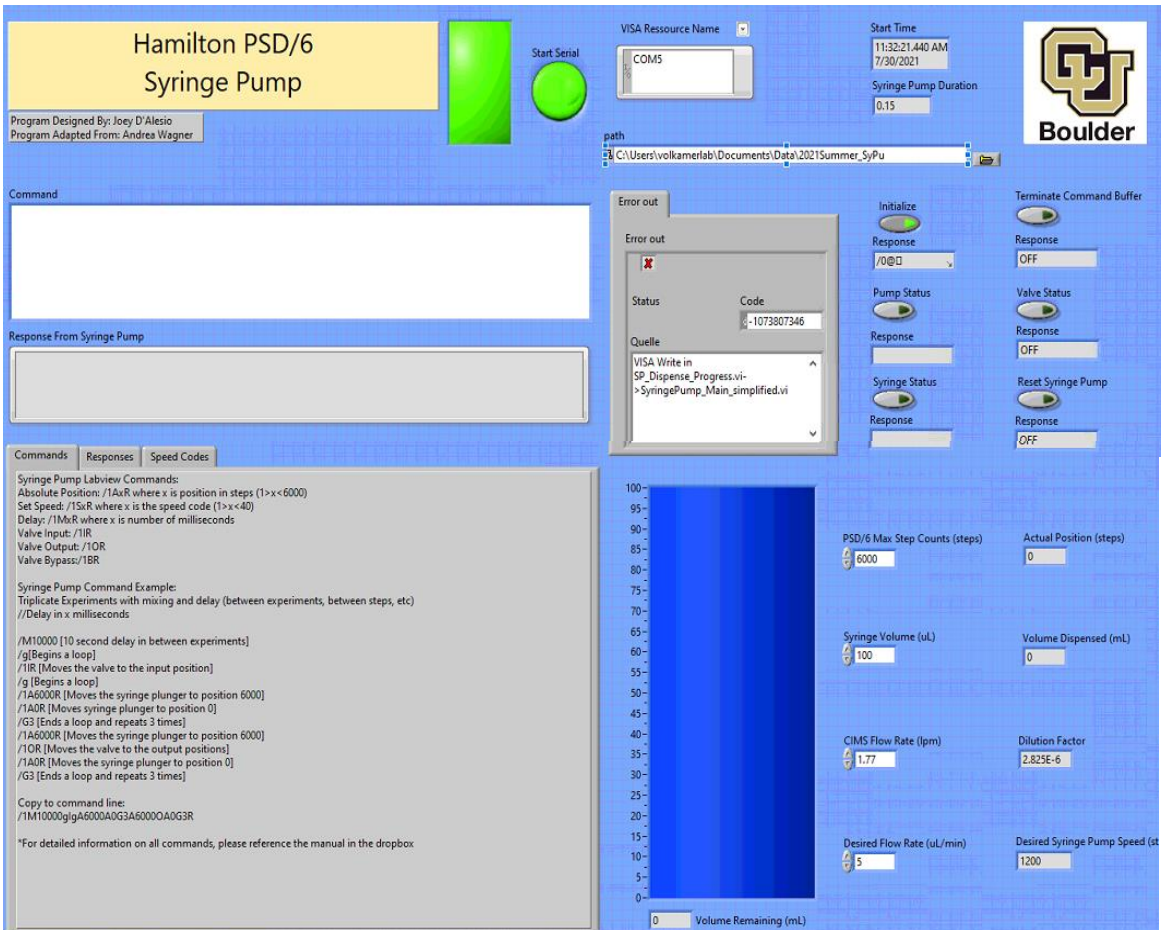

FIGURE 2.2: The Hamilton PSD/6 Syringe Pump graphical user interface (GUI) used to operate the pump and inject the aqueous sample into the setup during quantification experiments.

tested and optimized with cumene hydroperoxide. Cumene hydroperoxide was chosen because it is a nonpoisonous and nonexplosive hydroperoxide that is commercially available, it is stable in the aqueous and the gas phase, and it is detectable on a nominal mass for which no other peak is detected by the quadrupole. The overarching goal of the syringe pump optimization was to determine parameters that can reproducibility measure stable signal in the ppt-ppb range. The parameters that were optimized include the syringe pump flow rate, syringe volume, and external line heating temperature. The intention of this subsection is to briefly comment on what was

tested and optimized in order to document important parameters that are used in both the integration method and the flow rate method.

2.3.1 Flow Rate Optimization

Enthalpy of Vaporization for Investigated Compounds	
Compound	**Heat of Vaporization (J/kmol)**
Isoprene	2.73E+4 at 299 K
Cumene Hydroperoxide	6.99E+7 at 298 K
Formic Acid	2.96E+4 at 303 K
Acetic Acid	4.16E+4 at 304 K
Hexanoic Acid	6.84E+4 at 313 K
Heptanoic Acid	7.25E+4 at 306 K
Caprylic Acid	8.00E+4 at 290 K
Ethylene Glycol	6.19E+4 at 273 K
Glyoxylic Acid	4.20E+4 at 305 K
Malonic Acid	9.20E+4 at 296 K
Succinic Acid	5.73E+4 at 416 K

TABLE 2.1: The enthalpy of vaporization for compounds measured in this work [23] [24] [25] [26] [27] [28] [29] [30] [31] [32] [33].

The flow rate refers to the volume of liquid dispensed in microliters from the syringe pump per unit of time in minutes. As it has a direct effect on the evaporation rate of the sample under investigation, the flow rate was the first parameter optimized. The enthalpy of vaporization or the heat of evaporation is the energy needed to transform a liquid substance into its gaseous form. Every compound has a unique enthalpy of vaporization (Table 2.1). For these experiments, the desired flow rate should be less than or equal to the rate of evaporation for a compound. A flow rate that is less than

the rate of evaporation ensures that there will be constant evaporation of the liquid sample and thus a constant flow of gas analyte into the CIMS inlet. Additionally, this flow rate prevents the formation of a puddle (a buildup of sample in the t-piece and the lines). The formation of puddles introduces another surface into and out of which gas molecules can partition. Partitioning affects the measurement of gas molecules at the inlet due to the time it takes a compound to partition into and out of a puddle. Essentially, the presence of a puddle would equate to measuring less gas molecules at the time of evaporation and more gas molecules when there is no sample left to evaporate. It was determined that a flow rate within the range of 5–15 uL/min was optimal as it was slightly less than the compound's evaporation rate. Furthermore, a flow rate within this range provides a quantifiable gas-phase signal and it is supported by the available concentration and volume regimes. Water was the chosen solvent for all of the measured sample solutions. As such, water was used to optimize initial flow rate testing. While water is not visible in the CIMS spectrum on its own, this was not a problem for 4 reasons: 1) the reagent ion (iodide) clusters with water, 2) water is readily available to work with, 3) water did not dirty the Teflon lines, and 4) the syringe pump was disconnected from the CIMS inlet during initial evaporation testing. By having an open setup, it was possible to observe droplet and puddle formation in an open air environment. Once an optimal flow rate was achieved with water in an open air environment, the syringe pump was reconnected to the setup in order to take advantage of the humidified N_2 air stream intended for calibration. Droplet and puddle formation were checked after the entire sample volume had been dispensed into the lines during the closed environment testing. As flow rate has the largest effect on evaporation, the optimization of the other parameters was informed by the flow rate optimization.

2.3.2 Syringe Volume Optimization

Figure 2.3 provides the volume of the syringe in uL, the set speed and the actual speed in steps/second, the injection time in minutes, and the flow rate in uL/min. The actual speed is the number of steps (the entire volume of a syringe is defined as 6000 steps) the syringe pump will move per second. Upon initial testing and observation, it was discovered that the speed command issued to the syringe pump must be set to twice the actual speed desired. Thus, the set speed is the command issued to the syringe pump in order to achieve the "actual" or desired speed. Syringe size optimization was informed by the optimized flow rate in addition to the preferred injection time. An optimal injection time depends upon the stability of the gas-phase signal. Ultimately, the determination of a calibration coefficients and a Henry's Law coefficients is dependent upon measuring enough stable signal on which to perform an average. For these experiments, the LTOF-CIMS is set to collect an entire mass spectrum every second. With this collection setting, 15 minutes of stable signal offers sufficient statistics to calculate an average. Of course, a longer runtime leads to better statistics and a more accurate average. When considering the sample runtime, one must account for the time it takes the sample to equilibrate the lines. Line equilibration time refers to the time it takes for the sample to adsorb in and desorb out of the Teflon lines until an equilibrium is reached. Line equilibration time was measured on the order of 7 minutes following sample injection and following the completion of sample evaporation.

2.3.3 Line Heating Optimization

Omega Heating wire is wrapped around the Teflon lines from where humidified water generates the humidifier air that is flowed over the sample, around the t-piece that houses the sample droplet, and then all the way to the pinhole of the CIMS. The

Flow Rate Range (uL/min)	Volume (uL)	Stroke Length (Steps)	Set Vx (Steps/second)	Actual Vx (steps/second)	Time (min)	Flow Rate
Min (1)	100	6000	2	1	100	1
5	100	6000	10	5	20	5
7.5	100	6000	15	7.5	13	7.5
10	100	6000	20	10	10	10
12.5	100	6000	25	12.5	8	12.5
15	100	6000	30	15	7	15
Max (5000)	100	6000	10000	5000	0	5000
Flow Rate Range (uL/min)	**Volume (uL)**	**Stroke Length (Steps)**	**Set Vx (Steps/second)**	**Actual Vx (steps/second)**	**Time (min)**	**Flow Rate**
Min (2.5)	250	6000	2	1	100	2.5
5	250	6000	4	2	50	5
7.5	250	6000	6	3	33	7.5
10	250	6000	8	4	25	10
12.5	250	6000	10	5	20	12.5
15	250	6000	12	6	17	15
Max (12500)	250	6000	10000	5000	0	12500
Flow Rate Range (uL/min)	**Volume (uL)**	**Stroke Length (Steps)**	**Set Vx (Steps/second)**	**Actual Vx (steps/second)**	**Time (min)**	**Flow Rate**
Min (5)	500	6000	2	1	100	5
5	500	6000	2	1	100	5
7.5	500	6000	3	1.5	67	7.5
10	500	6000	4	2	50	10
12.5	500	6000	5	2.5	40	12.5
15	500	6000	6	3	33	15
Max (25000)	500	6000	10000	5000	0	25000
Flow Rate Range (uL/min)	**Volume (uL)**	**Stroke Length (Steps)**	**Set Vx (Steps/second)**	**Actual Vx (steps/second)**	**Time (min)**	**Flow Rate**
Min (10)	1000	6000	2	1	100	10
5	1000	1500	2	1	25	10
7.5	1000	6000	-	-	-	-
10	1000	6000	2	1	100	10
12.5	1000	6000	-	-	-	-
15	1000	6000	3	1.5	67	15
Max (50000)	1000	6000	10000	5000	0	50000

FIGURE 2.3: Syringe pump operation parameters: the volume of the syringe in uL, the set speed and the actual speed in steps/second, the injection time in minutes, and the flow rate in uL/min.

heating wire not only aids in the evaporation of the sample but also increases the passivation and depassivation rates into the Teflon walls, allowing for faster overall run times. During optimization, the 5%, 10%, and 15% settings were tested. The heating wire had no observed effect on run times when set to higher than 15% or 50 °C. Therefore, the 15% setting was chosen as the optimal experimental setting.

2.4 Gas-Phase Quantification Methods and Data Analysis

2.4.1 The Integration method

The first method discussed, referred to throughout the thesis as "the integration method", is used to determine the Henry's Law coefficient for 1,2-ISOPOOH. The samples of 1,2-ISOPOOH used in this work were provided by collaborators Dr. Joel A. Thornton (University of Washington) and Dr. Zhenfa Zhang (University of North Carolina). The 1,2-ISOPOOH samples were stable in water upon sample preparation. However, stable gas-phase signals were not observed utilizing the syringe pump setup with the optimized parameters and a steady sample injection via the pump. The hypothesized reason for the observed unstable gas-phase signals is the use of water as a solvent. When utilizing the flow rate method, the water evaporates before the 1,2-ISOPOOH evaporates. Once the 1,2-ISOPOOH begins to evaporate, the compound is no longer in solution with water, and as such, the concentration varies throughout evaporation as less of the compound remains. With this observed evaporation behavior, a constant syringe pump flow rate cannot be used to quantify the gas signals for 1,2-ISOPOOH in solution with water. While it would be possible to achieve a stable signal with another solvent, Henry's Law coefficients are generally defined with water as the solvent. Additionally, the 1,2-ISOPOOH samples used in the liquid-phase analysis and in the partitioning experiments were solutions with water as the solvent. Thus, in order to use the quantified gas-phase signals to determine a Henry's Law coefficient, an integration approach was taken in which the entire defined volume was dispensed into the t-piece, creating a sample droplet. Humidified N_2 gas was then passed over the sample droplet to evaporate the 1,2-ISOPOOH entirely and to transport the gas sample into the CIMS inlet. With the integration method, the syringe pump flow rate is no longer a necessary parameter, and the runtime depends on when the signal returns to

the baseline established before injection.

2.4.2 The Flow Rate Method

The second method, referred to throughout the thesis as "the flow rate method" is used to determine preliminary calibration coefficients for a suite of acids during calibration tests for the TI^{3}GER campaign. The flow rate method utilizes all of the parameters described in section 2.3 and relies upon a constant injection flow rate in which a defined volume is injected into the t-piece to be evaporated and carried into the CIMS. Following the arrival of the LTOF-CIMS and the experiments with 1,2-ISOPOOH, it was determined that further method development was required to achieve a stable signal with the flow rate method and the chosen compounds. A working hypothesis was that the water in the sample droplet was evaporating faster than the compound of interest, essentially concentrating the compound in the droplet. The evaporation of this droplet would lead to a decrease in the droplet concentration, resulting in a variable signal. In order to ensure constant evaporation of the droplet, glass wool was added in the t-piece to increase the surface area by which the droplet could evaporate. A stable signal was achieved with the addition of the glass wool. However, a disadvantage to using glass wool is the introduction of a large surface area with potential memory effects. Ultimately, it is important to note that the determining factor for which method to use is how well the analyte evaporates with the solvent. If the analyte and the solvent evaporate completely separate from each other, the integration method should be used. If the analyte and the solvent evaporate together or one simply slightly faster than the other, the flow rate method should be used.

2.4.3 Data Analysis Procedures

Mass spectrums and accompanying data is acquired by the TOF in hour-long H5 files, with data collected every second. These files are then averaged to 10 seconds within Tofware, allowing for smaller files to keep on hand and to load within Tofware for pre-analysis. Pre-analysis consists of mass calibration, defining a reference spectrum, refining the baseline, refining the peak width and shape, integrating all of the files, and then normalizing the traces. The specifics of these processes can be found in the appendix. After pre-analyzing the data with Tofware, one can output fitted and integrated time series.

2.4.4 Normalization Procedures

Normalization accounts for instrument sensitivity. By normalizing to species that are assumed constant throughout the measurement period, one can distinguish between changes in signal and changes in instrument sensitivity. Because ion-molecule reactions rely on the number of reagent ions available to react, normalization is also a method by which depletion of the reagent ion is accounted for. Each time series is normalized to the reagent ion (I-), the reagent ion water cluster (H_2O I-), and the reagent ion dopant cluster (acetonitrile I-). Using the logarithmic formula presented in equation 2.1, reagent ion changes smaller than 10% lead to only a negligible deviation.

$$Normalized\ Ion = log(1 + \frac{Ion\ Signal}{I-\ Signal + H_2O\ I-\ Signal + Acetonitrile\ I-\ Signal}) \tag{2.1}$$

2.4.5 Background Subtraction Procedures

Data is recorded before the injection of a species into the CIMS inlet in order to establish the background for a certain mass. When discussing backgrounds, it is important to distinguish between chemical and non-chemical backgrounds. Chemical backgrounds include the instrument and line backgrounds. The instrument and line backgrounds are the signals detected by the instrument when a blank is measured. The procedure established for background subtraction relies on averaging the data across a stable time series for a minimum of 15 minutes in order to establish enough statistics to get a good average. This average background signal is then subtracted from the measurements. A non-chemical background would include the baseline of the TOF, which is subtracted during data analysis in Tofware. Ultimately, the total background is an amalgamation of many things (a species hanging around in the lines, a species present in the air or a species that shares a nominal mass with the species of interest, etc.) Regardless of the source, it is important to characterize the background so that the detected signal is representative of the targeted species.

2.5 Determination of a Henry's Law Coefficient for 1,2-ISOPOOH

2.5.1 The Integration Method Calibration Coefficient

The integration method utilizes an integration based approach to obtain the signal in normalized counts. The theory behind this integration approach is to account for all of the signal generated by the injected sample volume. To accomplish this, a baseline is established prior to the injection of the sample droplet into the Teflon t-piece. The total normalized counts detected by the CIMS is found by taking an area (equation 2.2) between the signal and the time elapsed from the injection of the droplet to the return

of the signal to the baseline.

$$Area \ = \ Signal \ x \ Time \tag{2.2}$$

During the integration method, the entire sample is injected into the t-piece and evaporated as humidified N_2 gas is passed over the sample. In order to ensure that no dirt or room air is sampled by the inlet, the total flow into the inlet is set to be greater than what will be accepted by the CIMS. For these experiments, the total flow into the inlet is set to be 2.03 slpm. Once the CIMS inlet cannot accept more flow, the overflow is output to a vent between the sample injection site (the t-piece) and the CIMS inlet. In order to determine the actual flow accepted into the CIMS inlet, a Gilibrator calibrator was used to measure the overflow at the vent. The overflow was measured to be .501 slpm. As such, it is important to consider the gas molecules lost at the vent by incorporating a dilution factor (equation 2.3) in the calculation.

$$Dilution \ Factor = \frac{Total \ Flow \ - \ Vent \ Flow}{Total \ Flow} = \frac{2.03 - 0.501}{2.03} = 0.753 \tag{2.3}$$

The dilution factor under these conditions is found to be .753. This means that approximately 75% of gas molecules formed from evaporating the aqueous sample actually enter the CIMS. The gas-phase concentration of 1,2-ISOPOOH (equation 2.4) can be determined by multiplying the aqueous-phase concentration by the determined dilution factor. A calibration coefficient in normalized counts per molecule can then be determined by plotting the normalized counts detected by the CIMS against the gas

molecules injected into the CIMS and finding the slope.

$$Gas\ Concentration = \ Aqueous\ Concentration\ x\ Dilution\ Factor \tag{2.4}$$

2.5.2 The Quantification of Gas-Phase Signals

Once the normalized counts detected per gas molecule injected (a calibration coefficient) is known for a particular compound, a gas-phase signal of the same compound measured on the same instrument can be quantified (equation 2.5). This is the heart and driving purpose of the syringe pump application.

$$Gas\ Molecules\ Sampled\ = \ \frac{Molecules}{Normalized\ Counts}\ x\ Gas\ Phase\ Signal \tag{2.5}$$

Once the number of gas molecules sampled is quantified for a gas-phase signal, a gas-phase concentration in one second can be expressed as molecules/cm3. As shown in equation 2.6, the gas molecules sample is divided by the volume the gas-phase occupies upon evaporation, where 0.8 L/min is the flow rate of the humidified N_2 gas over the sample.

$$\frac{Gas\ Molecules}{Volume} = \frac{Gas\ Molecules\ Sampled}{\frac{0.8\ L}{min}\ x\ \frac{1\ min}{60\ s}\ x\ \frac{1000\ cm^3}{1\ L}} \tag{2.6}$$

A partial pressure (equation 2.7) for the gas-phase compound of interest can then be determined by dividing the gas-phase concentration as determined above by the concentration of air molecules present at the time of measurement, defined at 273 K and 1 atm to be 2.5e19 molecules/cm^3.

$$Partial\ Pressure\ =\ \frac{Concentration\ Gas}{Concentration\ Air}\ x\ 1\ atm \tag{2.7}$$

Henry's Law coefficients for 1,2-ISOPOOH (equation 2.8) can then be determined in conjunction with a liquid phase analysis in which peroxide groups are quantified using an iodometric-spectrophotometric method [34]. The Henry's Law coefficient is defined as the aqueous concentration in M over the partial pressure of the gas in atm.

$$Henry's\ Law\ Coefficient\ =\ \frac{Aqueous\ Concentration}{Partial\ Pressure} \tag{2.8}$$

2.6 The Flow Rate Method Calibration Coefficient

The flow rate method utilizes a constant injection flow of the sample into the t-piece in order to establish a constant gas-phase signal at the CIMS inlet. A constant gas-phase signal allows for a time average of a stable region of signal as opposed to integrating the total signal in order to determine a calibration coefficient. During the flow rate method, a defined volume of sample is injected into the t-piece where it is evaporated and then carried via N_2 gas into the inlet every second. A noteworthy difference between the integration method and the flow rate method is the loss of molecules at the vent. The vent is positioned downstream from the droplet injection point and upstream from the CIMS inlet for both methods. With the flow rate method, the concentration of the aqueous sample is constant during evaporation, meaning that the concentration of the gas-phase sample entering the inlet is also constant. This means that the concentration of gas-phase sample measured at the inlet is representative of the concentration upstream from the vent; only volume is lost at the vent. As such,

the number of gas molecules sampled per second (equation 2.9) is found using the aqueous sample concentration in M, the flow rate in L/s, and Avogadro's number.

$$Gas\ Molecules\ Sampled\ =\ Aqueous\ Concentration\ x\ Flow\ Rate\ x\ Avogadro's\ Number \quad (2.9)$$

The gas-phase concentration (equation 2.10) in one second expressed as molecules /cm^3 can be determined by dividing the number of gas molecules by the volume the gas-phase occupies upon evaporation, where 2.0 L/min is the flow rate of the humidified N_2 gas over the sample.

$$\frac{Gas\ Molecules}{Volume} = \frac{Gas\ Molecules\ Sampled}{\frac{2.0\ L}{min}\ x\ \frac{1\ min}{60\ s}\ x\ \frac{1000\ cm^3}{1\ L}} \quad (2.10)$$

Once the gas-phase concentration is known, a mixing ratio (equation 2.11) by mass can be calculated by dividing the gas-phase concentration by the concentration of air molecules. This ratio can be multiplied by 10x where x could be 6 for parts-per-million (ppm), 9 for parts-per-billion (ppb), or 12 for parts-per-trillion (ppt).

$$Mixing\ Ratio\ =\ \frac{Gas\ Concentration}{Air\ Concentration}\ x\ 10^x \quad (2.11)$$

The gas-phase signal detected by the CIMS can then be plotted against the gas-phase concentration. The slope of this plot will be the calibration coefficient in normalized counts per second (ncps) per concentration unit (ppm, ppb, ppt, etc.).

3 Results and Discussion

3.1 Syringe Pump Optimization

Table 3.1 displays the experimental conditions for the syringe pump optimization experiments. As described above in the methods section, these experiments were performed on a quadrupole CIMS with cumene hydroperoxide. The experiments focused on the aqueous concentration of cumene hydroperoxide in mM, the injection flow rate in uL/min, the heating wire temperature setting in %, the injection runtime in minutes, the presence of a droplet following injection, the presence of a puddle following injection, and the average counts detected by the CIMS. The goal of these experiments is to determine settings that will provide a stable signal without a remaining droplet or puddle following the injection. Essentially, the syringe pump settings should evaporate the sample at a rate that is faster than the sample is injected into the setup. The rows in red represent settings that resulted in either a droplet, a puddle, or both. The rows in green represent settings that resulted in no droplet or puddle, and are thus optimal settings for experiments moving forward.

The settings used to perform the experiment displayed in Figure 3.1 are those presented in the last row of Table 3.1 (70 mM cumene hydroperoxide solution, 10 uL/min injection flow rate, 10% heating wire setting). As shown in Figure 3.1, the cumene hydroperoxide signal measured by the CIMS is stable for almost 3 hours, more than enough time to find the total average signal in normalized counts.

When similar settings (4 mM cumene hydroperoxide solution, 10 uL/min injection flow rate, 10% heating wire setting) are applied to 1,2-ISOPOOH using the TOF-CIMS as displayed in Figure 3.1, a stable signal is not achieved. As such, the integration method is used to determine the total average signal in normalized counts.

Syringe Pump Optimization Experimental Table						
Cumene Concentration (mM)	Flow Rate (uL/min)	Heating Wire Temperature Setting (%)	Injection Runtime (min)	Droplet	Puddle	Average Normalized Counts
35	10	5	100	yes	yes	205
35	15	5	67	no	yes	244
70	10	5	100	yes	yes	324
70	15	5	67	yes	no	252
35	10	10	100	no	no	160
35	15	10	67	no	no	259
70	10	10	100	no	no	288

TABLE 3.1: Experimental conditions for syringe pump optimization experiments. The rows in red represent settings that result in a sample puddle in the lines or a sample droplet suspended from the injection line. The rows in greed represent optimal settings in which the sample is fully evaporated.

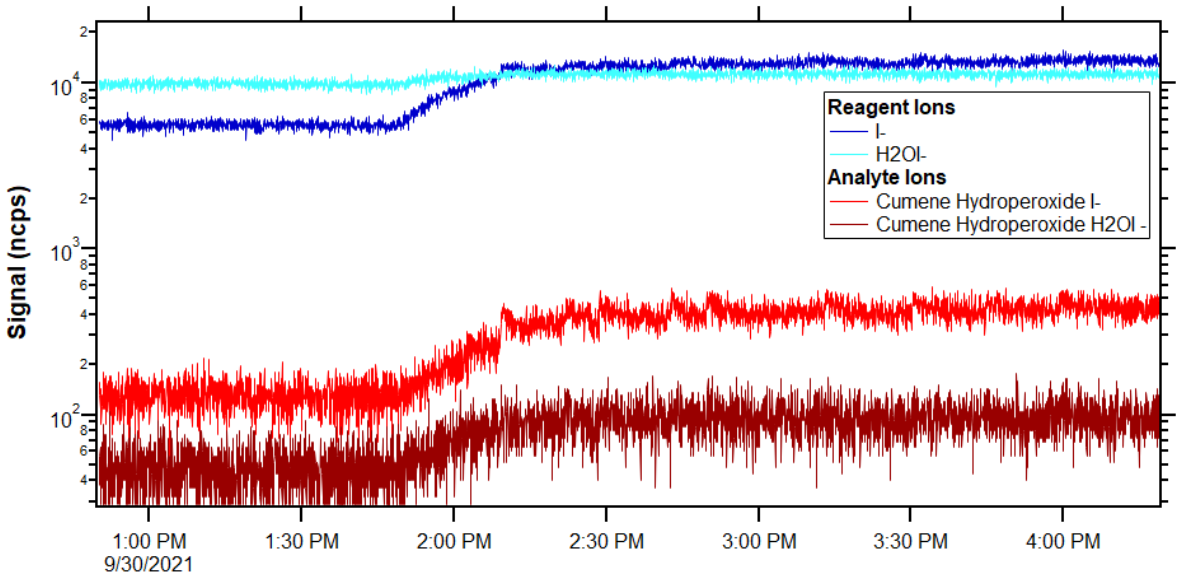

FIGURE 3.1: Optimal settings (70 mM cumene hydroperoxide solution, 10 uL/min injection flow rate, 10% heating wire setting) to achieve a stable signal utilizing the flow rate method measuring cumene hydroperoxide with a quadrupole CIMS.

It is worth noting that a significantly lower concentration of 1,2-ISOPOOH is used in these experiments as the ionization efficiency for 1,2-ISOPOOH is significantly greater than that of cumene hydroperoxide.

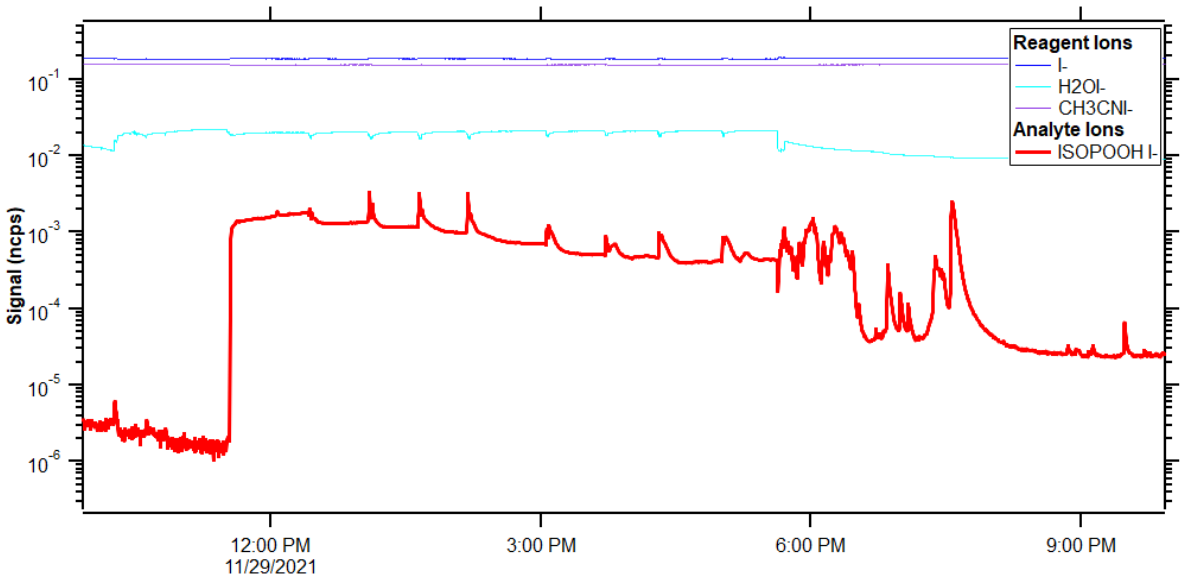

FIGURE 3.2: Stable signal is not achieved utilizing the flow rate method with settings that provided stable signal during the optimization experiments (4 mM cumene hydroperoxide solution, 10 uL/min injection flow rate, 10% heating wire setting) to measure 1,2-ISOPOOH with an LTOF-CIMS.

3.2 The Integration Method

3.2.1 The 1,2-ISOPOOH Calibration Coefficient

The calibration coefficient for 1,2-ISOPOOH was determined with the integration method. A droplet of the 1,2-ISOPOOH solution is dispensed into the setup and humidified N_2 gas is flowed over the sample to completely evaporate it. The resulting gas-phase sample is carried into the CIMS inlet and the corresponding signal is integrated from the pre-injection baseline until the signal returns to this established baseline. The integration procedure in Igor Pro used to determine the total signal in normalized

counts takes the integration from the signal timetrace to the line y=0. As the baseline for the 1,2-ISOPOOH signal is greater than 0 ncps, a correction is applied to all integrations. A trapezoid containing the area between the starting and stopping signal and y=0 is subtracted from the total determined signal. The integrated signals and the integration correction is displayed in Figure 3.3. The bounds of this integration are determined in order to capture the total signal and thus the total gas-phase molecules of 1,2-ISOPOOH injected into the CIMS from the known aqueous concentration.

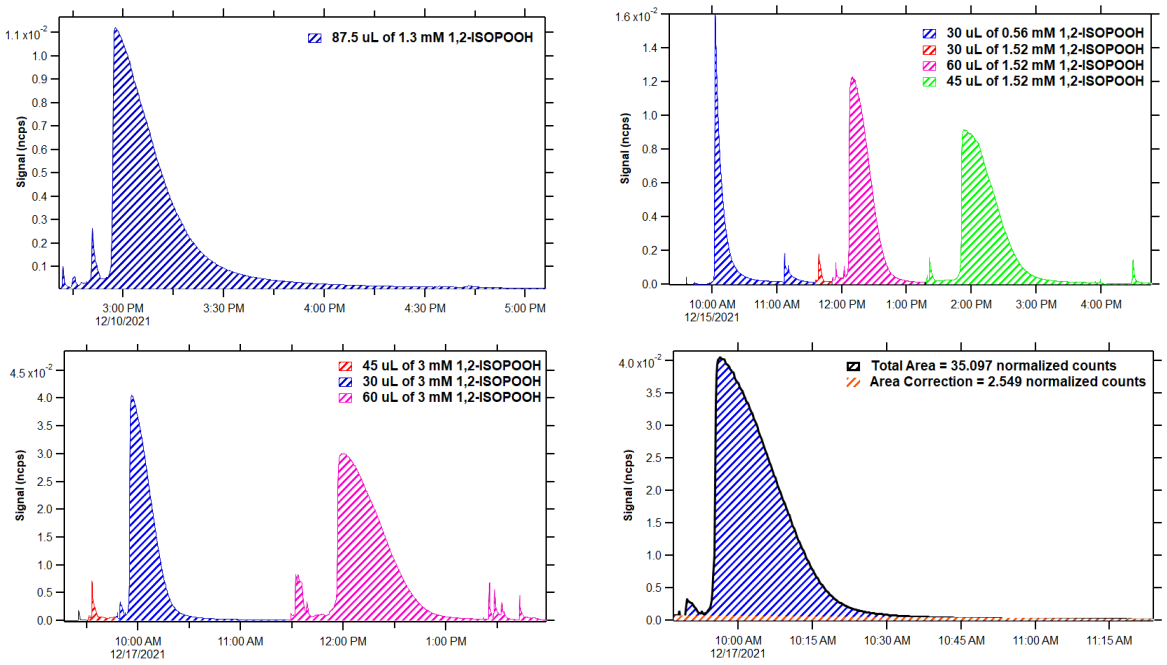

FIGURE 3.3: Gas-phase 1,2-ISOPOOH signals are integrated from the pre-injection baseline until the signal returns to the established baseline in order to determine the total gas-phase 1,2-ISOPOOH molecules were injected into the CIMS on December 10th, 2021 (top left), December 15th, 2021 (top right) and December 17th, 2021 (bottom left). The area correction (bottom right) is shown in orange to correct for integrated signal between y=0 and the signal baseline.

As displayed in Figure 3.3, the 1,2-ISOPOOH signal reaches an inflection point before a somewhat exponential decay. It is hypothesized that the water in the injected

sample droplet is evaporating at a faster rate than the 1,2-ISOPOOH, resulting in a concentrated 1,2-ISOPOOH droplet. As the 1,2-ISOPOOH evaporates, this concentration decreases and the signal detected by the CIMS also decreases. As displayed in Table 3.2, this method is reproducible across different aqueous-phase concentrations of 1,2-ISOPOOH and different sample droplet volumes. These integration measurements represent the lower end of the gas-phase 1,2-ISOPOOH molecules injected in the CIMS as the signals were not integrated entirely to the baselines established pre-injection. Since the signal decayed exponentially as it returned to the baseline, it was not reasonable to wait until the baseline returned to the exact starting baseline. While the difference between the starting and ending baselines are negligible, it is worth noting that potential loss in signal. There are two experimental runs (shown in red on December 15th and December 17th) in which the CIMS detected a significantly lower signal than expected. Both of these outlier points had a total runtime of approximately 15 minutes as opposed to the normal runtime of 1-2 hours. Interestingly enough, both outlier points are also on the same order of magnitude. Table 3.2 displays the experimental conditions for the determination of 1,2-ISOPOOH calibration coefficients. The salting flask integration method is a variation of the syringe pump integration method. Randall Chiu, a graduate student in the Volkamer group, ran similar experiments to determine a calibration coefficient for 1,2-ISOPOOH. Instead of using the syringe pump setup and injecting the sample into a t-piece as described in the methods section, Chiu injected a 10 uL 1,2-ISOPOOH sample into the round bottom flask used in the partitioning experiments. As in the syringe pump integration method, N_2 gas was flowed over the aqueous sample to evaporate it and then carry the gas-phase molecules into the CIMS inlet. The gas-phase 1,2-ISOPOOH molecules injected into

the CIMS and the resulting signals in normalized counts are reported in the table below along with the aqueous-phase concentrations in mM, sample volumes in uL, and the N_2 flow rate in slpm.

Calibration Constant Experiment Table for 1,2-ISOPOOH						
Method	**Measurement Day**	**Aqueous-Phase Concentration**	**Sample Volume**	**N_2 Flow Rate**	**Signal (normalized counts)**	**Gas-Phase Molecules**
Syringe Pump Integration Method	December 15, 2021	0.56 mM	30.0 uL	2.03 slpm	7.21	7.63E+15
	December 15, 2021	1.52 mM	45.0 uL	2.03 slpm	15.54	4.14E+16
	December 15, 2021	1.52 mM	60.0 uL	2.03 slpm	19.80	3.10E+16
	December 17, 2021	3.00 mM	45.0 uL	2.03 slpm	32.55	4.08E+16
	December 17, 2021	3.00 mM	60.0 uL	2.03 slpm	57.86	8.17E+16
Salting Flask Integration Method	December 14, 2021	0.562 mM	10.0 uL	2.30 slpm	0.021	2.12E+13
	December 15, 2021	0.562 mM	10.0 uL	2.30 slpm	1.47	2.12E+15
	December 17, 2021	3.00 mM	10.0 uL	2.30 slpm	2.41	2.83E+15
	December 18, 2021	3.00 mM	10.0 uL	2.30 slpm	3.99	2.83E+15
	December 19, 2021	3.00 mM	10.0 uL	2.30 slpm	22.37	1.13E+16

TABLE 3.2: Experimental conditions for the measurement of 1,2-ISOPOOH gas-phase signal utilizing the integration method with the syringe pump setup and the salting flask setup.

At this time, it is unknown what may have caused a loss in the total number of gas-phase 1,2-ISOPOOH molecules injected. It is possible that there may have been air bubbles present in the lines when dispensing the sample droplet into the t-piece. If this were the case, the total number of aqueous-phase 1,2-ISOPOOH molecules would be lower resulting in less gas-phase molecules detected by the CIMS. It is also possible that the 1,2-ISOPOOH was still evaporating when the next run was initiated. However, this is not likely: there was time after the red traces returned to the baseline and before the next injection was initiated, and the integrations following these

"outlier" runs are consistent with the other measurements. When these two "outlier" measurements are excluded from the dataset, the signal or the total normalized counts detected by the CIMS increases with the gas-phase 1,2-ISOPOOH molecules injected as expected.

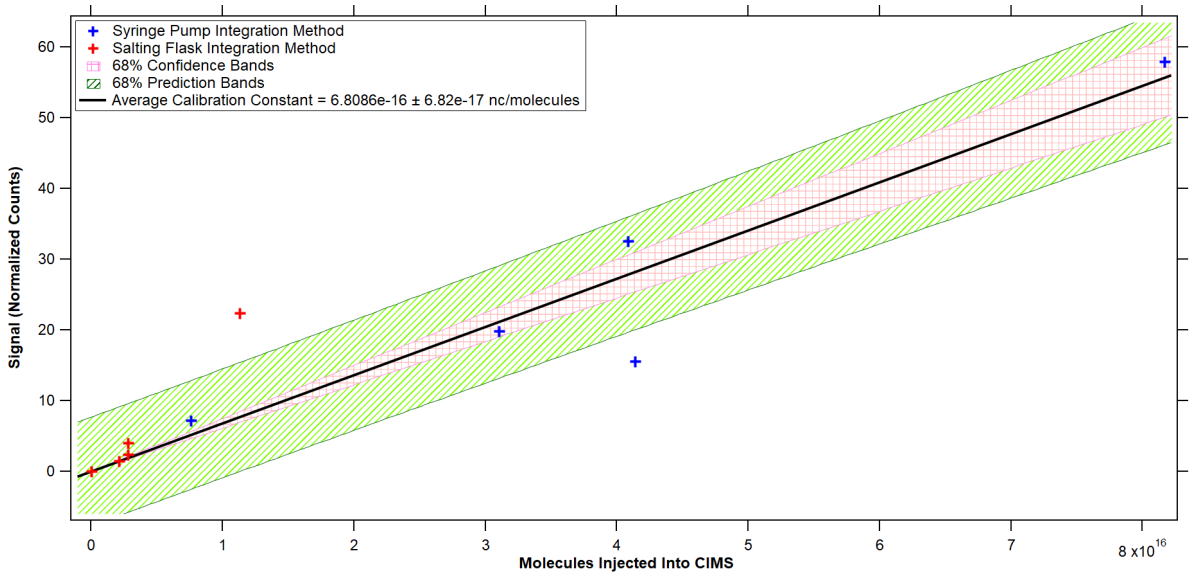

FIGURE 3.4: 1,2-ISOPOOH gas-phase signal detected vs 1,2-ISOPOOH gas-phase molecules injected into the CIMS for the syringe pump integration method (blue) and the salting flask integration method (red). The 1,2-ISOPOOH calibration coefficient is found to be 6.81e-16 normalized counts/molecules or 1.47E+15 molecules/normalized counts.

Figure 3.4 displays the detected signal in normalized counts vs the 1,2-ISOPOOH gas molecules injected into the CIMS inlet for the syringe pump integration method (blue) and the salting flask integration method (red). The slope of this plot is the calibration coefficient (black line) and is found to be 6.81e-16 normalized counts/molecules or 1.47E+15 molecules/normalized counts. The cross-hatch region of the plot (pink) is the 68% confidence band and expresses sampling uncertainty. The striped region of the plot (green) is the 68% prediction band. Prediction bands account for the uncertainty in the estimation of the population mean as well as the random variation of

the individual sampled values. As such, prediction bands will always be wider than confidence bands. All of the data points except for two fall within the 68% prediction band; half of the data points are within the 68% confidence band. The two points that fall outside of the one sigma band fall within two sigma from the fit.

3.2.2 The 1,2-ISOPOOH Henry's Law Coefficient

The calibration coefficient determined above, 1.47E+15 molecules/normalized counts, is used to quantify gas-phase 1,2-ISOPOOH signals measured with the same LTOF-CIMS in order to determine a Henry's Law coefficient. The gas-phase 1,2-ISOPOOH signals chosen for quantification were measured during partitioning experiments. The partitioning experiments performed with 1,2-ISOPOOH are focused on understanding how the addition of a salt (ammonium sulfate and sodium oxalate in this case) affects the partitioning of 1,2-ISOPOOH between the gas and aqueous phase. At the beginning of every partitioning measurement day, two to three 1,2-ISOPOOH samples containing no salt were measured in order to determine a baseline signal from which to determine if the salts affected partitioning.

Table 3.3 displays the measurement days, detailing the aqueous-phase concentrations and the corresponding gas-phase signals detected by the CIMS. As described above in the methods section, the 1,2-ISOPOOH calibration coefficient is then applied to the no salt 1,2-ISOPOOH gas-phase signals in order to determine Henry's Law coefficients for 1,2-ISOPOOH in M/atm where M refers to the molarity of the aqueous-phase 1,2-ISOPOOH concentration and atm refers to the partial pressure of the gas-phase 1,2-ISOPOOH. The 1,2-ISOPOOH Henry's Law coefficients are displayed in Figure 3.5.

Henry's Law Constant Experiment Table for 1,2-ISOPOOH			
Measurement Day	**Aqueous-Phase Concentration (mM)**	**Gas-Phase Signal (normalized counts)**	**Henry's Law Constants (M/atm)**
November 24, 2021	0.4500	0.000259	2.65E+05
November 24, 2021	0.4500	0.000340	3.12E+05
November 29, 2021	0.9389	0.000503	2.91E+05
November 29, 2021	0.9389	0.000427	2.08E+05
November 29, 2021	0.9389	0.000458	1.94E+05
November 30, 2021	0.4150	0.000284	2.80E+05
November 30, 2021	0.4150	0.000304	2.07E+05
December 13, 2021	0.5624	0.000286	2.39E+05
December 13, 2021	0.5624	0.000386	3.31E+05
December 13, 2021	0.5624	0.000335	2.80E+05
December 02, 2021	0.8650	0.000372	2.96E+05
December 02, 2021	0.8650	0.000439	2.50E+05
December 02, 2021	0.8650	0.000416	2.24E+05
December 03, 2021	1.2500	0.000711	2.82E+05
December 03, 2021	1.2500	0.000793	2.83E+05
December 08, 2021	1.2988	0.000654	2.49E+05
December 08, 2021	1.2988	0.000653	2.98E+05
December 08, 2021	1.2988	0.000740	2.70E+05
December 14, 2021	1.5195	0.000724	2.89E+05
December 14, 2021	1.5195	0.000801	2.47E+05
December 14, 2021	1.5195	0.000748	1.88E+05

TABLE 3.3: The 1,2-ISOPOOH Henry's Law coefficients determined by applying the integration method calibration coefficient to the gas-phase 1,2-ISOPOOH partitioning data from the above measurement days.

This study reports the 1,2-ISOPOOH Henry's Law coefficient to be 2.61E+05 M/atm, which falls within the range of values reported throughout literature. Rivera Rios reports the 1,2-ISOPOOH Henry's Law coefficient to be 1.18e+05 M/atm. Rivera Rios evaporated 10 mL of 103 mM aqueous-phase 1,2-ISOPOOH from a round bottom flask with an air flow, sampling the gas-phase molecules with a CF_3O- CIMS. Ranventos-Duran reports the 1,2-ISOPOOH Henry's Law coefficient to be 7.53E+05 M/ATM. The EVAPORATION+AIOMFAC model reports the 1,2-ISOPOOH Henry's Law coefficient to be 1E+05 M/atm. The GROMHE model reports the 1,2-ISOPOOH

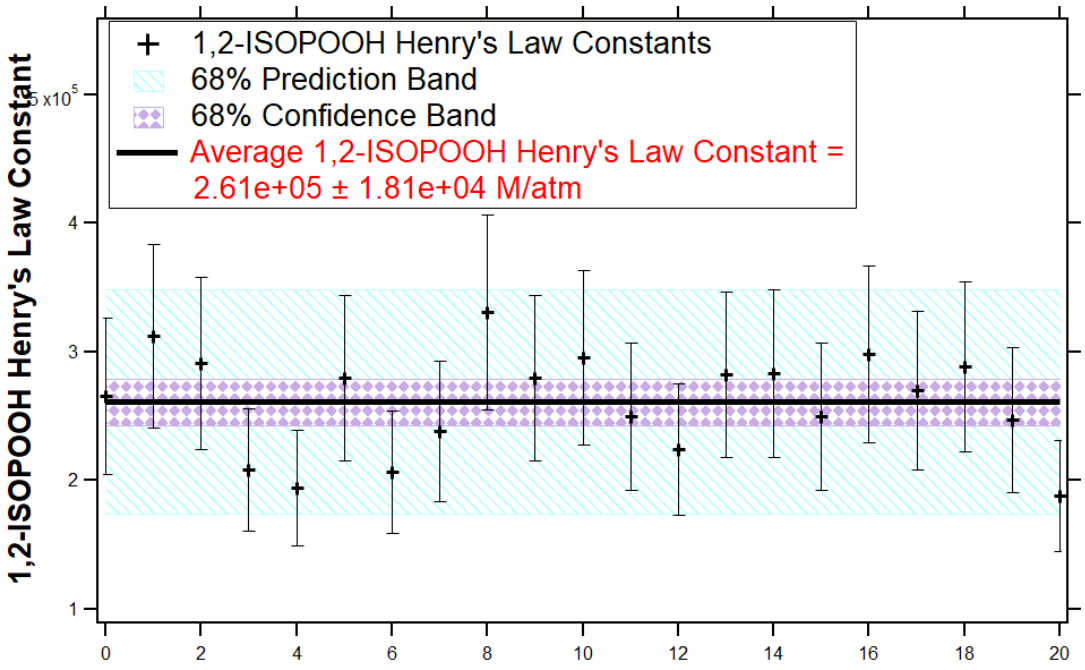

FIGURE 3.5: The measured 1,2-ISOPOOH Henry's Law coefficients. The black crosses represent the measured Henry's Law coefficient for each partitioning measurement containing no salt. The purple dotted band is the 68% confidence band, and the blue striped band is the 68% prediction band. All of the measured Henry's coefficients fall within one sigma from the average or within the 68% prediction band. The average 1,2-ISOPOOH Henry's Law coefficient (black line) is 2.61E+05 +/- 1.81E+04 M/atm.

Henry's Law coefficient to be 1.3E+05 M/atm. These values are summarized in Table 3.4. Figure 3.6 depicts the Henry's Law coefficient determined in this study alongside the values reported in literature.

The high value for the 1,2-ISOPOOH Henry's Law coefficient, as measured in this study, suggests that 1,2-ISOPOOH is likely to partition to cloud water, and possibly even aerosol water. This means that like glyoxal, methylglyoxal, and IEPOX, 1,2-ISOPOOH is likely to be absorbed by cloud droplets, fog waters, or aqueous aerosol particles and react to form aqSOA [8].

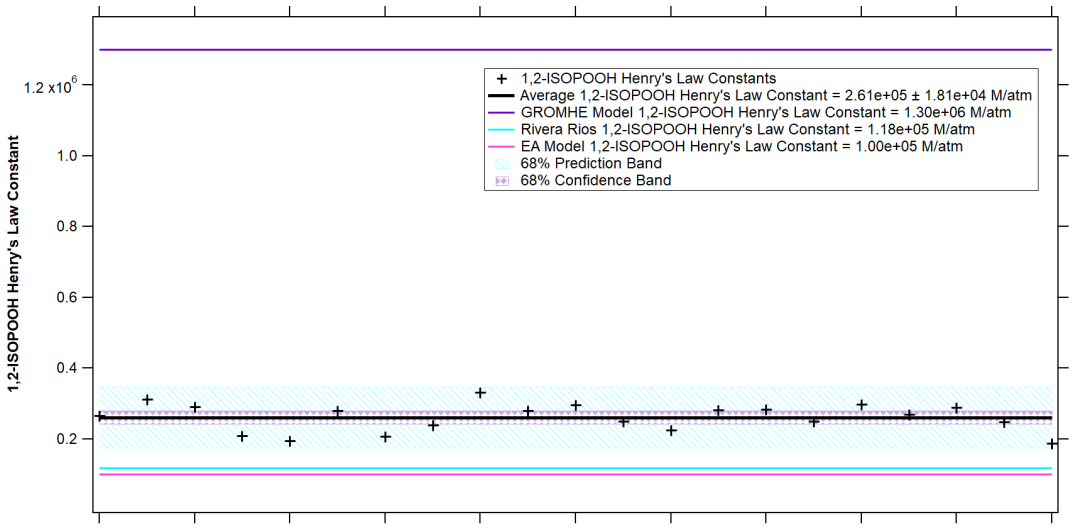

FIGURE 3.6: A literature comparison for the 1,2-ISOPOOH Henry's Law Coefficient.

Summary of 1,2-ISOPOOH Henry's Law Constants (M·atm−1)			
This Study KH 30°C	**Rios KH 25°C**	**E + A 25 °C**	**GROMHE 25 °C**
2.61E+05	1.18E+05	1.00E+05	1.30E+06

TABLE 3.4: A Summary of 1,2-ISOPOOH Henry's Law Coefficient reported in literature.

3.3 The Flow Rate Method

3.3.1 Characterizing Atmospherically Relevant Calibration Compounds

This section is focused on the application of the flow rate method during initial calibration testing for the TI^{3}GER aircraft campaign. The calibration testing performed in this work provides an initial characterization of the Tofwerk LTOF mass spectrometer combined with the VOCUS AIM ion source in iodide mode before the instrument was

re-racked for the aircraft. Between the time the 1,2-ISOPOOH experiments were performed with the integration method and the initial calibration testing began, a stable signal was achieved with the flow rate method. As such, the flow rate method was used for initial calibration testing. Documentation of this calibration application for the flow rate method is documented in the appendix of this thesis for future use in the laboratory and the field. One of the goals of this preliminary calibration was to determine the range of ionization efficiencies capable on this instrument. As such, ionization efficiency was a major factor considered when choosing the standards with which to calibrate. Ultimately, "calibration cocktails" containing a suite of chemicals from fatty acids to dicarboxylic acids were tested and measured by the CIMS. After analyzing the dataset, the chosen compounds fell into two distinct categories: "compounds that evaporate with their solvent" and "compounds that evaporate after their solvent". The "compounds that evaporate with their solvent" include formic acid, ethylene glycol, caprylic acid, heptanoic acid, hexanoic acid, and acetic acid. These compounds were generally determined to have lower backgrounds and linear calibration curves. All of these compounds contain a carboxylic acid group except for Ethylene Glycol, which has two alcohol groups. These acids display a constant signal upon injection into the syringe pump setup. As displayed in Figure 3.7, these compounds reach a period of stability about 7 minutes after injection and remain stable for approximately 15-20 minutes, allowing for enough time to time-average the signal. The "compounds that evaporate after their solvent" include glyoxylic acid, malonic acid, succinic acid, and oxalic acid. These compounds all experience a behavior in which there is low to no signal in the presence of water and exponentially decaying signal in the absence of water. All of these compounds contain two carboxylic acid groups except for glyoxylic acid, which has a carboxylic acid group and an aldehyde group. Upon injection of the

calibration cocktail into the syringe pump setup, no to minimal signal is initially detected by the CIMS. Once the "compounds that evaporate with their solvent" return to their baseline signals, a signal is detected by the CIMS for the "compounds that evaporate after their solvent".

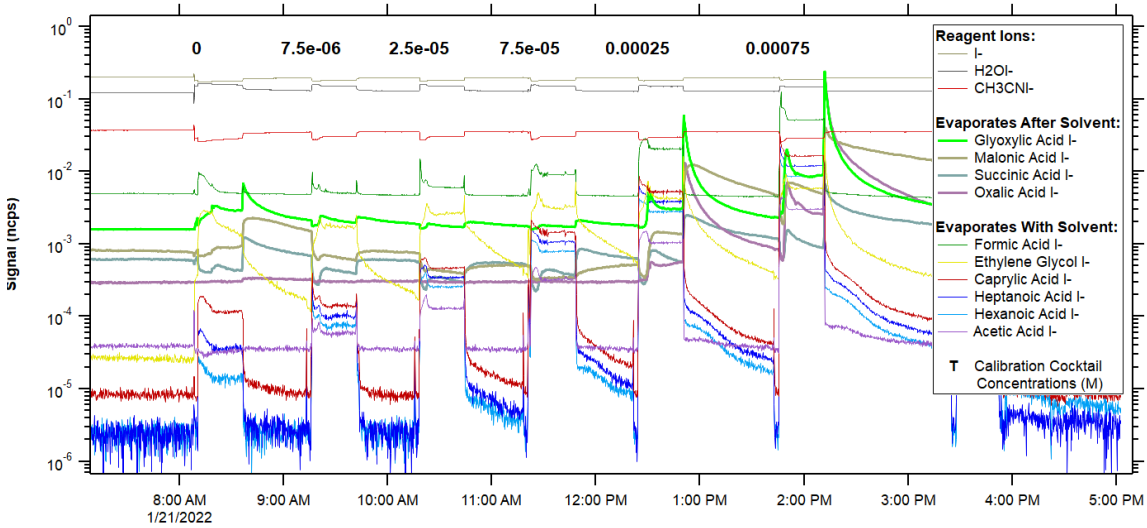

FIGURE 3.7: A time series from January 21st, 2022 of the compounds chosen to measure during initial calibration testing for the Tofwerk LTOF CIMS. The compounds can be categorized based on their observed behavior as "compounds that evaporate with their solvent" and "compounds that evaporate after their solvent".

Figure 3.7 is a time series from January 21st, 2022. Although initial calibration measurements were taken throughout the entire month of January, this time series in particular will be analyzed in depth throughout this thesis. The addition of glass wool on the 19th, 20th, and 21st allowed for stable signal and thus the determination of preliminary calibration coefficients with the flow rate method. Of the three days with stable signal utilizing the flow rate method, the measurements taken on the 21st have lower backgrounds than the those completed on the 19th and 20th. The syringe pump setup lines were exposed to room air on the morning of the 19th when the clean carrier gas was running low, causing higher backgrounds through the 20th.

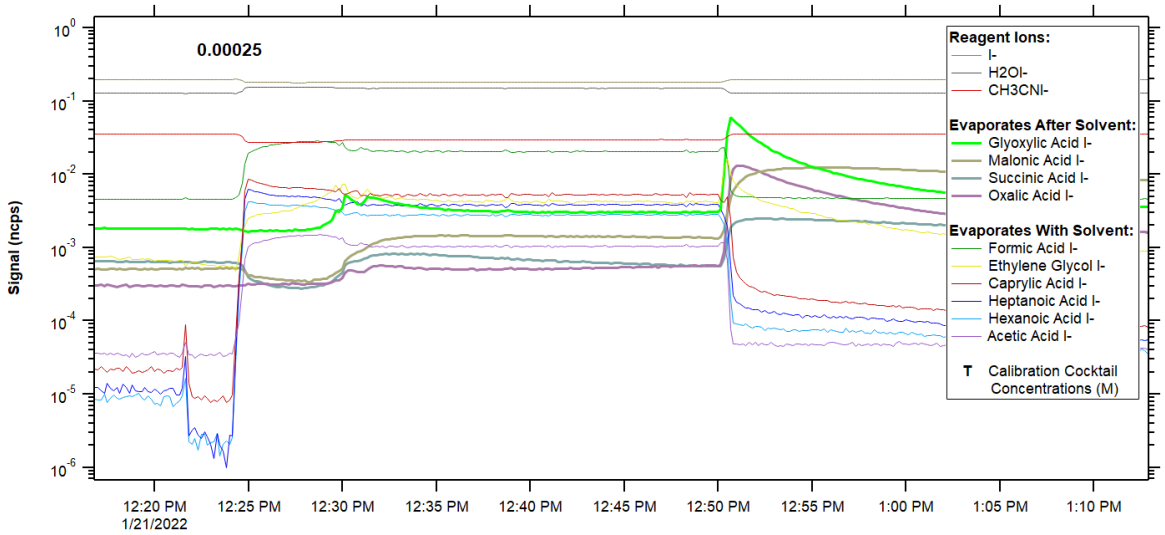

FIGURE 3.8: A syringe pump injection from the start to the end on January 21st, 2022. The injection begins around 12:23 pm and ends around 12:53 pm. The "compounds that evaporate with their solvent" are stable during the injection period. The "compounds that evaporate after their solvent" peak and decay following the end of the injection.

Figure 3.8 displays a syringe pump injection (zoomed in from Figure 3.7) from start to end. The injection begins around 12:23 pm and ends around 12:53 pm. During the period in which the syringe pump is actively injecting sample into the setup, the "compounds that evaporate with their solvent" reach stability. At 12:53 pm, after the syringe pump has completed the sample injection into the lines, the signal for the "compounds that evaporate after their solvent" begins to peak and decay. As such, the two categories of compounds exhibit distinct behaviors.

3.3.2 Reagent Ion Depletion

The reagent ions used for the calibration experiments include I-, H_2OI-, and Acetonitrile I-. Reagent ion depletion is seen above in Figure 3.9. At the start of the day, the I-

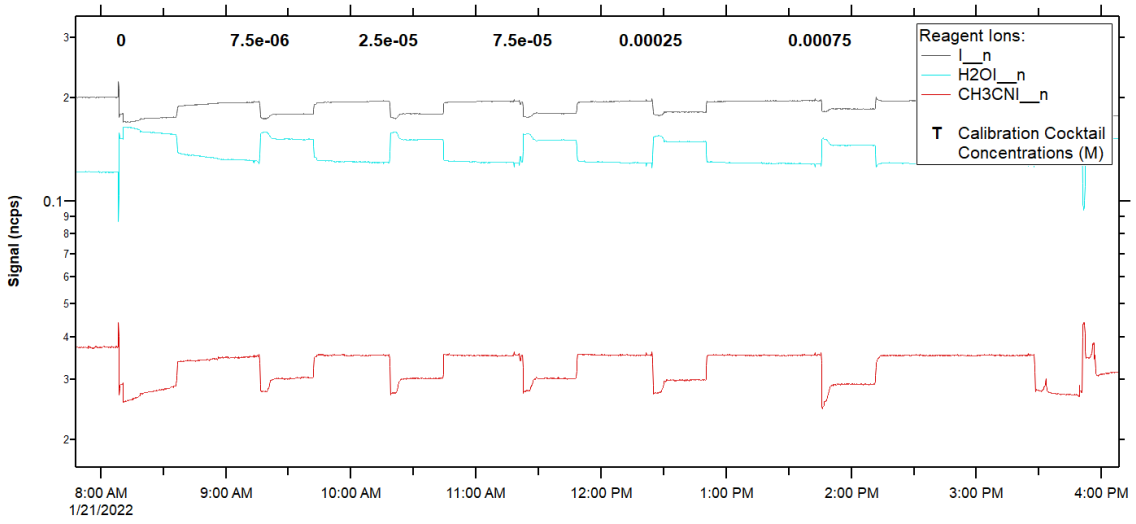

FIGURE 3.9: The preliminary calibration experiments utilized an AIM ion source with an I- reagent scheme. In total, I-, H_2O I-, and Acetonitrile I- are defined as reagent ions. During the evaporation of the "compounds that evaporate with their solvent", the I- signal depleted 13%, the H_2O I- signal increased 30%, and the Acetonitrile I- signal depleted 24%. During the evaporation of the "compounds that evaporate after their solvent", the I- signal depleted 4.5%, the H_2O I- signal increased 8.9%, and the Acetonitrile I- signal depleted 6.7%.

signal was 0.2014 ncps, the H_2OI- signal was 0.1209 ncps, and the Acetonitrile I- signal was 0.03704 ncps. During the evaporation of the "compounds that evaporate with their solvent", the I- signal depleted 13% to 0.1751 ncps. The H_2OI- signal increased 30% to 0.1572 ncps. The Acetonitrile I- signal depleted 24% to 0.02783 ncps. During the "compounds that evaporate after their solvent", I- depleted 4.5% to 0.1923 ncps. The H_2OI- signal increased 8.9% to 0.1317 ncps. The Acetonitrile I- signal depleted 6.7% to 0.03455 ncps. The reagent ions do change throughout the experimental runs, more so for the "compounds that evaporate with their solvent" than the "compounds that evaporate after their solvent". This is not surprising as the former group is evaporating with the solvent, which in this case is water, and water is taking the reagent ions away from I- to form the H_2O I- cluster. Thus, most of the I- depletion is due to

the presence of water and appears in the observed increase in the H_2O I- signal.

3.3.3 Compounds That Evaporate After Their Solvent

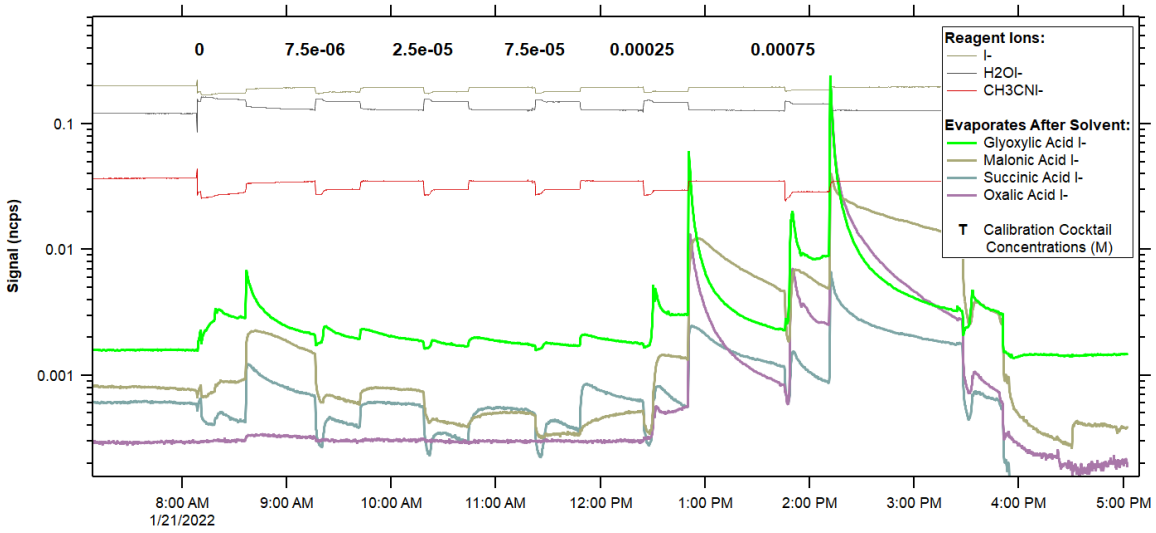

FIGURE 3.10: The "compounds that evaporate after their solvent" are observed to peak in signal following the completion of the syringe pump injection and thus following the evaporation of water. Instead of reaching stability, the signals follow different exponential decays.

The "compounds that evaporate after their solvent" do not reach stability as observed for the "compounds that evaporate with their solvent". Instead, the compounds follow a general exponential decay behavior. Malonic and succinic acids observe similar behavior patters as do glyoxylic and oxalic acids. This makes sense as succinic acid (two carboxylic acid groups) is essentially the same structure as malonic acid (with two carboxylic acid groups) with an additional CH_2 in between the functional groups. Succinic and malonic acids also have very similar backgrounds. Oxalic Acid (with two carboxylic acid groups) is essentially the same structure as glyoxylic acid (with a carboxylic acid group and an aldehyde group) with an aditional OH group. However, oxalic and glyoxylic acids have very different backgrounds. The

CIMS detects a higher background signal for glyoxylic acid, which means that more ions are formed between glyoxylic acid and iodide than between oxalic acid and iodide.This makes sense with the replacement of an aldehyde group for a carboxylic acid group, as the acid group is less reactive due to its electron conjugation. Less reactive groups ultimately have lower backgrounds due to a lower ionization efficiency, which is a major driver for sensitivity.

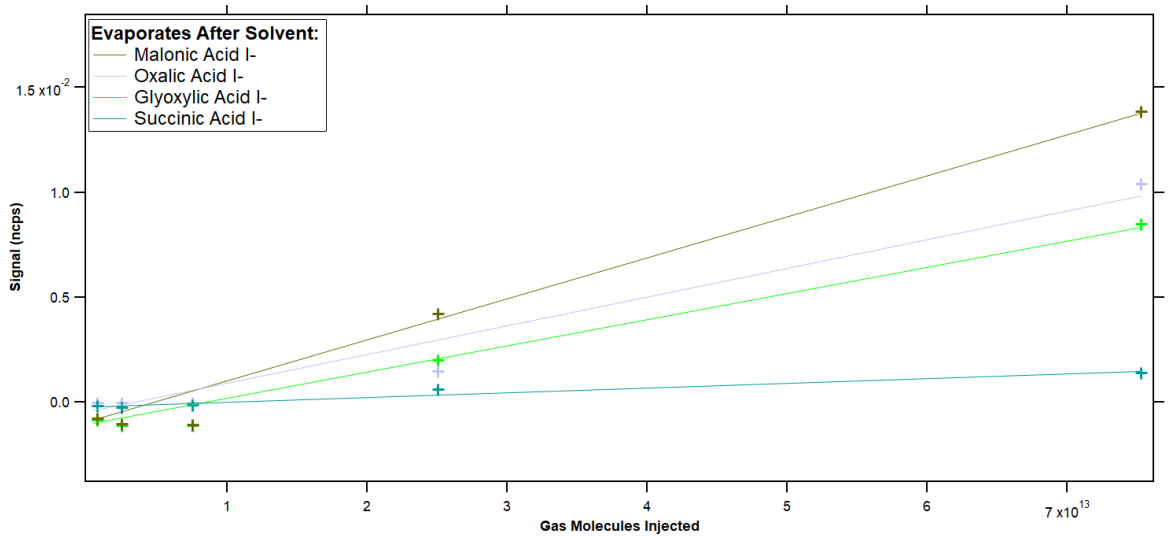

FIGURE 3.11: The measured signal (ncps) vs the gas molecules injected into the CIMS inlet for the "compounds that evaporate after their solvent". A decrease in signal is observed for the first three experiments as the number of gas molecules injected is increased. The subsequent experiments display an increase in signal with an increase in gas molecules injected.

While it is expected that the signal detected by the CIMS would increase as the concentration of the compounds injected increases, this is not observed for the first three concentrations of the "compounds that evaporate after their solvent". This can be seen in Figure 3.11. The first three runs seem to decrease in signal or remain somewhat constant in signal as the concentration is increased. In fact, it appears that the siganls for malonic and succinic acid decrease below the baselines at one point while

glyoxylic and oxalic acid remain constant. However, the signals for the subsequent concentrations respond as expected: the signal increases as the gas molecules injected increases. There are many reasons this could be observed. It appears that the signals for all of the "compounds that evaporate after their solvent" were higher than the actual background at the start of the experiment. The subsequent injection and evaporation of the "calibration cocktail" appears to also evaporate compound that was already in the lines at the start of the experiment day. Prior to the start of the experiment day, the lines had been rinsed with water and were allowed 12+ hours to flush and equilibrate. Because these compounds do not evaporate with water, it is reccommended to flush the lines with a solvent with which these compounds will evaporate.

3.3.4 Compounds That Evaporate With Their Solvents

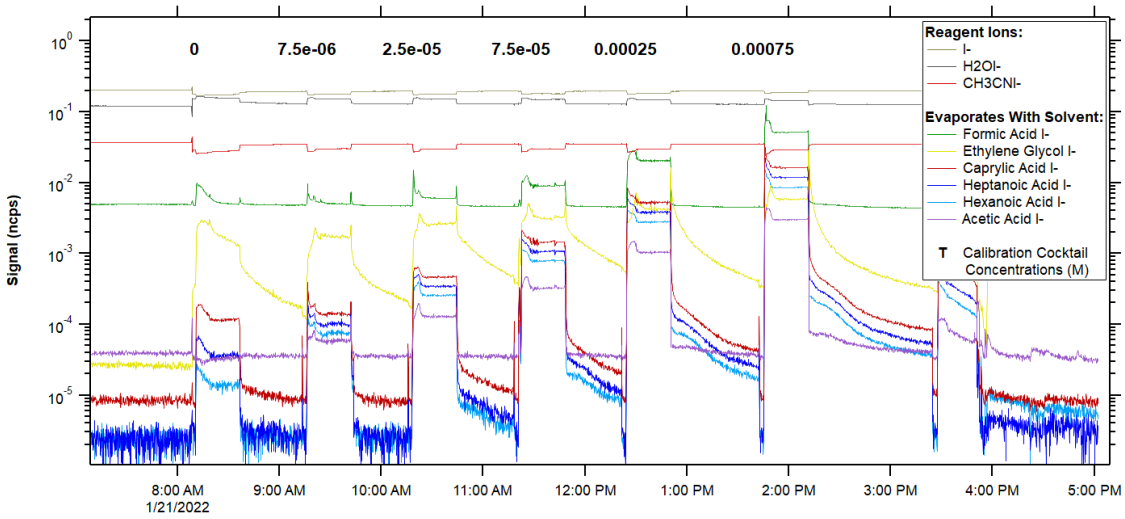

FIGURE 3.12: The "compounds that evaporate with their solvent" are observed to peak and reach stability approximately 7 minutes after the injection of the compounds into the setup. There appears to be a depassivation time following the completion of the injection that increases as the concentration of the "calibration cocktail" increases.

The "compounds that evaporate with their solvent" reach stability following a line passivation time of approximately 7 minutes after the start of injection. Following the completion of injection, there is an observed depassivation time that increases as the "calibration cocktail" concentration injected increases. In comparing the backgrounds of the "compounds that evaporate with their solvent", formic acid has the highest background followed by acetic acid, ethylene glycol, caprylic acid, hexanoic acid, and then heptanoic acid. Formic acid is the simplest carboxylic acid, having just one carbon atom. Before any formic acid has been introduced into the syringe pump setup or the CIMS, the signal is still on the order of 10^{-3} ncps, which is higher than expected for an acid with this structure. It is speculated that there is a formic acid source somewhere in the ion source, as toluene is present in the iodide source and acetonitrile is used as the dopant. Acetic acid has the next highest background and is a step above formic acid in terms of simplicity, having just two carbon atoms in addition to the carboxylic acid group. Ethylene glycol, with two carbon atoms and two alcohol groups, has the next highest background. The alcohol groups do not have a carbonyl group for electron conjugation and are thus more reactive. Caprylic acid, also known as octonoic acid, has the next highest background with 8 carbon atoms and a carbonyl group. Hexanoic acid (6 carbon atoms with a carbonyl group) and heptanoic acid (7 carbon atoms) have almost identical backgrounds; however, hexanoic acid has a slightly higher background. Formic acid (also known as methanoic acid) and acetic acid (also known as ethanoic acid) behave similarly. Both compounds have a signal that spikes upon injection, stabilizes, and returns to the baseline. Hexanoic, heptanoic, and caprylic acids all behave the same. At the end of the syringe pump injection, the signal experiences an exponential decay back to the baseline. These are depassivation curves and represent the time it takes for the compounds to absorb in and desorb out

of the Teflon lines.

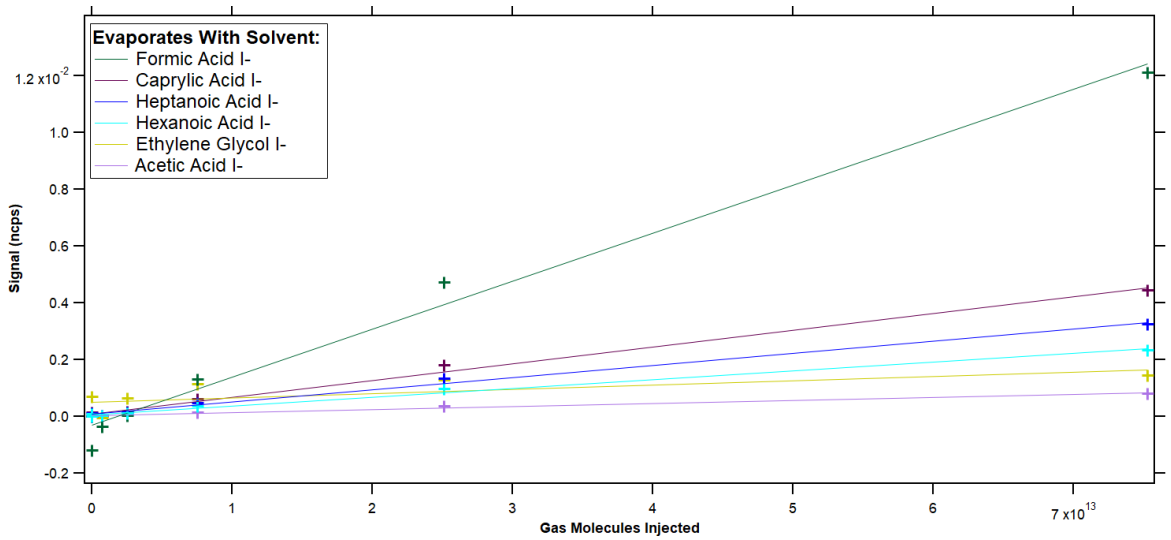

FIGURE 3.13: The measured signal (ncps) vs the gas molecules injected into the CIMS inlet for the "compounds that evaporate with their solvent". An increase in signal is observed as the number of gas molecules injected is increased.

For the "compounds that evaporate with their solvent", the measured signal increases as the gas molecules injected into the CIMS increases. A range of concentrations for each acid were measured in this study. As can be seen in Figure 3.13, there is a signal response for the initial zero concentration sample, containing just water. This signal is most likely representative of the acids remaining in the setup and the lines. This could explain the minimal signal detected after the addition of the first two samples (7.5e-6 M and 2.5e-05 M) despite what appear to be large peaks in Figure 3.12. Additionally, Figure 3.13 makes the case that the higher observed background is not related to higher sensitivity. The highest sensitivity observed is for formic acid, which does have the highest background. However, caprylic acid has the next highest sensitivity and the 3rd highest background. Heptanoic acid has the next highest sensitivity and the lowest background. This is important to note as it demonstrates that

sensitivity is independent of the background signal.

3.4 Preliminary Calibration coefficients for a Suite of Atmospherically Relevant Compounds

Each calibration compound was analyzed in depth using Tofware and Igor Pro 8. The analysis began by looking at the peaks present at each nominal mass to determine if there were any double peaks on the nominal masses of the chosen calibration compounds. If a double peak was present, this secondary peak was identified as an unknown peak within Tofware and subtracted from the peak of interest. Any secondary peaks are noted in the subsections below. Additionally, as the acetonitrile I- cluster was present at a lower concentration than anticipated during calibration measurements, potential H_2O I- and $(H_2O)_2$ I- clusters are noted for the calibration compounds. Finally, the average signals in normalized counts is plotted against the gas-phase concentration in molecules/cm^3 to determine a calibration coefficient in molecules/cm^3 for each compound.

3.4.1 The Characterization of Formic Acid

Formic acid or methanoic acid is the simplest carboxylic acid consisting of a carboxyl group. The formic acid iodide cluster has a nominal mass of 173. There are two peaks present at the nominal mass of 173: NO_2 I- and formic acid I-. The formic acid I- peak is present at around 4900 ions/s and the NO_2I- peak is present at 0 ions/s. The formic acid I- water cluster is also present in low quantities. The calibration curve for Formic Acid is presented in Figure 3.14. As one of the "compounds that evaporates with their solvent", Formic Acid has a linear curve with a calibration coefficient of

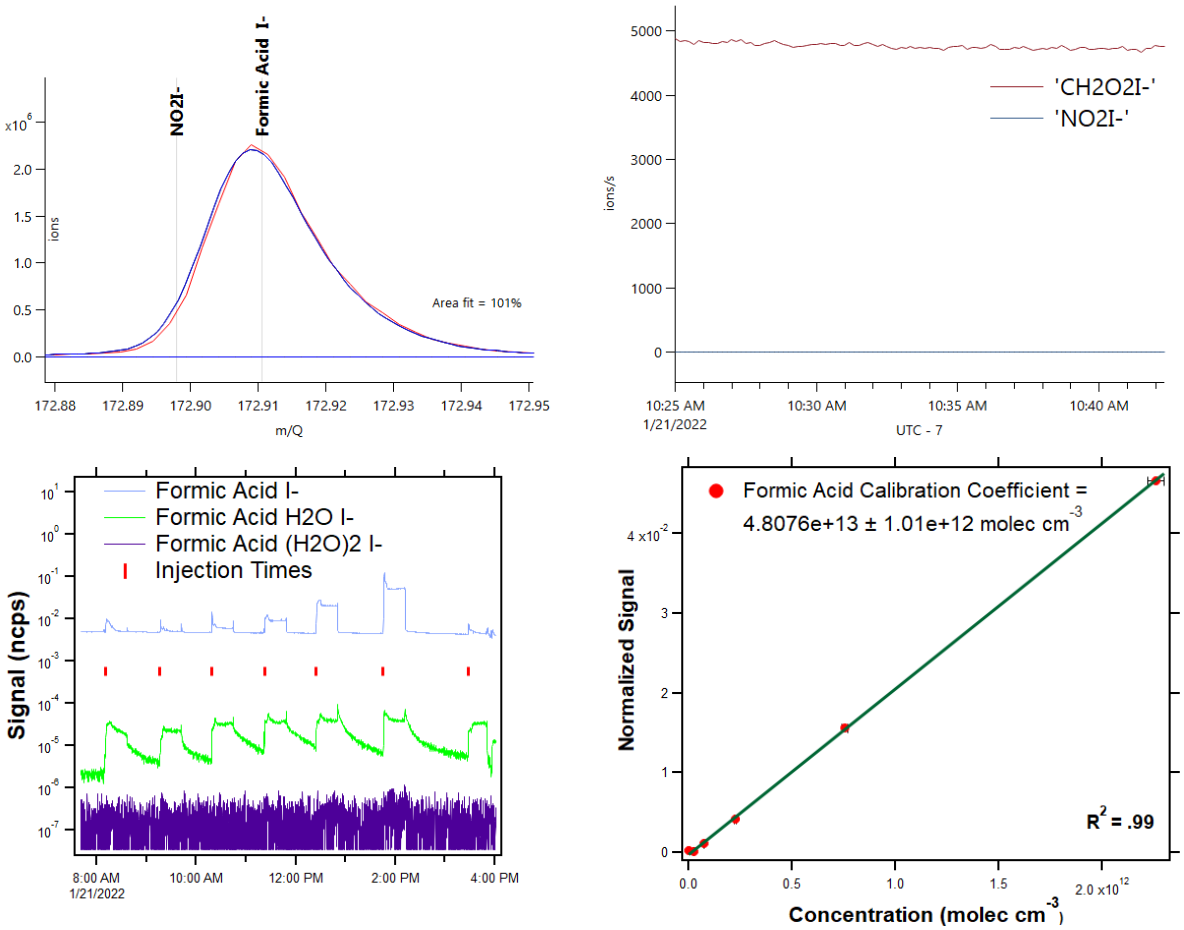

FIGURE 3.14: Characterization of formic acid: The detected formic acid I- peak shape at m/z=173 (top left), the time series of formic acid I- (top right), formic acid I- hydrates (bottom left), and the preliminary formic acid calibration coefficient of 4.81E+13 +/- 1.01E+12 molecules/cm^3.

4.81E+13 +/- 1.01E+12 molecules/cm^3 as displayed in the equation below. The y-intercept is congruent with zero within the error.

$$[CH_2O_2] \;=\; 4.8\; x\; 10^{13}\; molec.\; cm^{-3}\; x\; \frac{CH_2O_2 \cdot I^-}{(I^- + H_2O \cdot I^- + C_2H_3N \cdot I^-)} \tag{3.1}$$

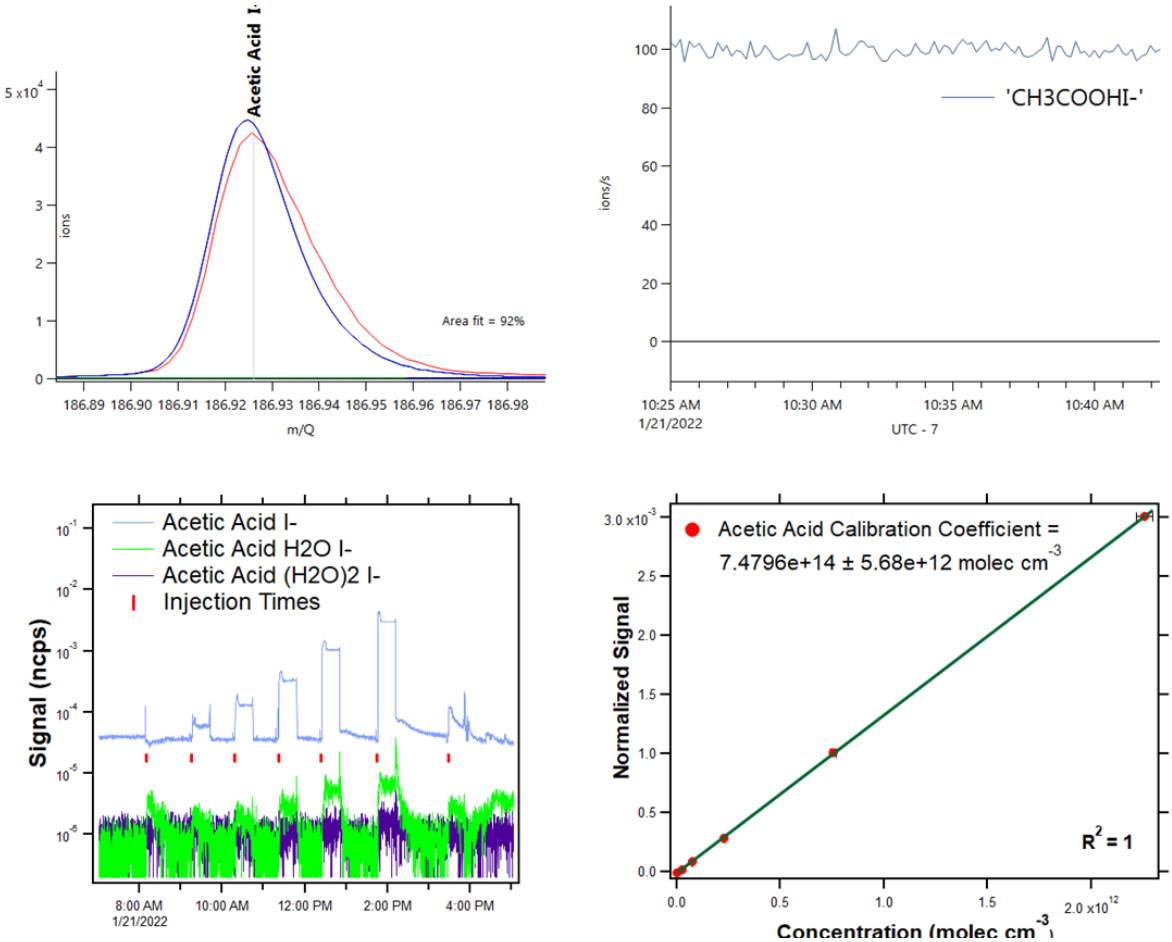

FIGURE 3.15: Characterization of acetic acid: The detected acetic acid I- peak shape at m/z=187 (top left), the time series of acetic acid I- (top right), acetic acid I- hydrates (bottom left), and the preliminary acetic acid calibration coefficient of 7.48E+14 +/- 5.68E+12 molecules/cm^3.

3.4.2 The Characterization of Acetic Acid

Acetic acid or ethanoic acid is the next simplest carboxylic acid with one carbon atom and a carboxyl group. The acetic acid iodide cluster has a nominal mass of 187 amu. Acetic acid is the only peak present at this nominal mass. The acetic acid I- peak is present at around 105 ions/s. The acetic acid I- water cluster is also present at low quantities. The calibration curve for acetic acid is presented in Figure 3.15. As one of the "compounds that evaporates with their solvent", acetic acid has a linear curve

with a calibration coefficient of 7.48E+14 +/- 5.68E+12 molecules/cm^3 as displayed in the equation below. The y-intercept is congruent with zero within the error.

$$[CH_3COOH] \; = \; 7.5 \; x \; 10^{14} \; molec. \; cm^{-3} \; x \; \frac{CH_3COOH \cdot I^-}{(I^- + H_2O \cdot I^- + C_2H_3N \cdot I^-)} \tag{3.2}$$

3.4.3 The Characterization of Hexanoic Acid

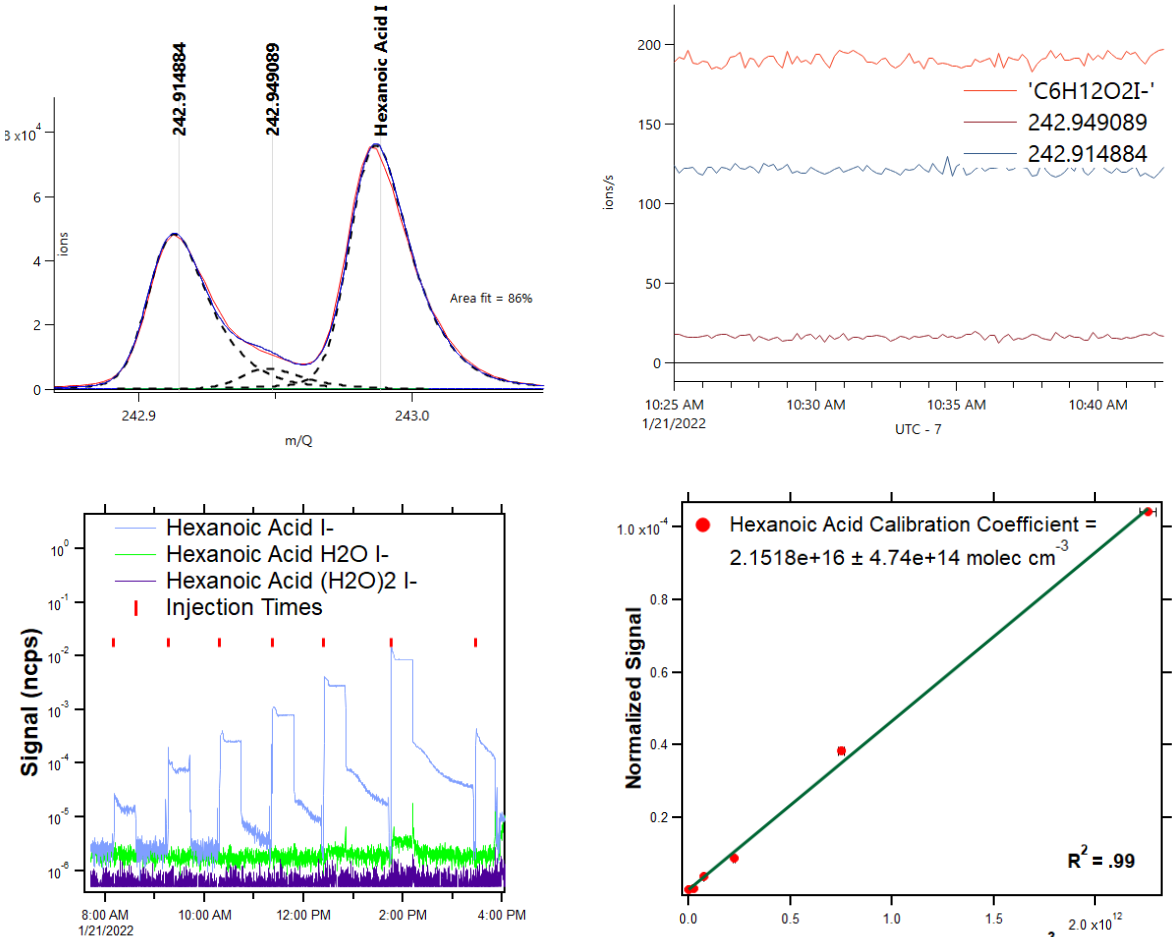

FIGURE 3.16: Characterization of hexanoic acid: The detected hexanoic acid I- peak shape at m/z=243 (top left), the time series of hexanoic acid I- (top right), hexanoic acid I- hydrates (bottom left), and the preliminary hexanoic acid calibration coefficient of 2.15E+16 +/- 4.74E+14 molecules/cm^3.

Hexanoic acid or caproic acid or is a carboxylic acid with five carbon atoms and a

carboxyl group. The hexanoic acid iodide cluster has a nominal mass of 243. There are three peaks present at the nominal mass of 243: hexanoic acid I-, an unknown peak at 242.914884 amu, and an unknown peak at 242.949089 amu. The hexanoic acid peak is present at 190 ions/s. The 242.914884 peak is present at 125 ions/s and the 242.949089 peak is present at 25 ions/s. The hexanoic acid I- water cluster is also present at low quantities. The calibration curve for hexanoic acid is presented in Figure 3.16. As one of the "compounds that evaporate with their solvent", hexanoic acid has a linear curve with a calibration coefficient of 2.15E+16 +/- 4.74E+14 molecules/cm^3 as displayed in the equation below.

$$[C_6H_{12}O_2] \;=\; 2.2\ x\ 10^{16}\ molec.\ cm^{-3}\ x\ \frac{C_6H_{12}O_2 \cdot I^-}{(I^- + H_2O \cdot I^- + C_2H_3N \cdot I^-)}\ - 2.8\ x\ 10^{-7} \tag{3.3}$$

3.4.4 The Characterization of Heptanoic Acid

Heptanoic acid or enanthic acid is a carboxylic acid with six carbon atoms and a carboxyl group. The heptanoic acid iodide cluster has a nominal mass of 257. There are five peaks present at the nominal mass of 257: heptanoic acid I-, an unknown peak at 257.019185 amu, an unknown peak at 256.895380 amu, an unknown peak at 256.965165 amu, and an unknown peak at 256.930471 amu. The heptanoic acid I- peak is present at 250 ions/s. The 257.019185 peak is present at 0 ions/s. The 256.895380 peak is present at 10 ions/s. The 256.965165 peak is present at 20 ions/s. The 256.930471 peak is present at 30 ions/s. The heptanoic acid water cluster is present at negligible quantities. The calibration curve for heptanoic acid is presented in Figure 3.17. As one of "compounds that evaporate with their solvent", heptanoic acid has a linear curve with a calibration coefficient of 1.49E+16 +/- 8.16E+14 molecules/cm^3 as displayed in the

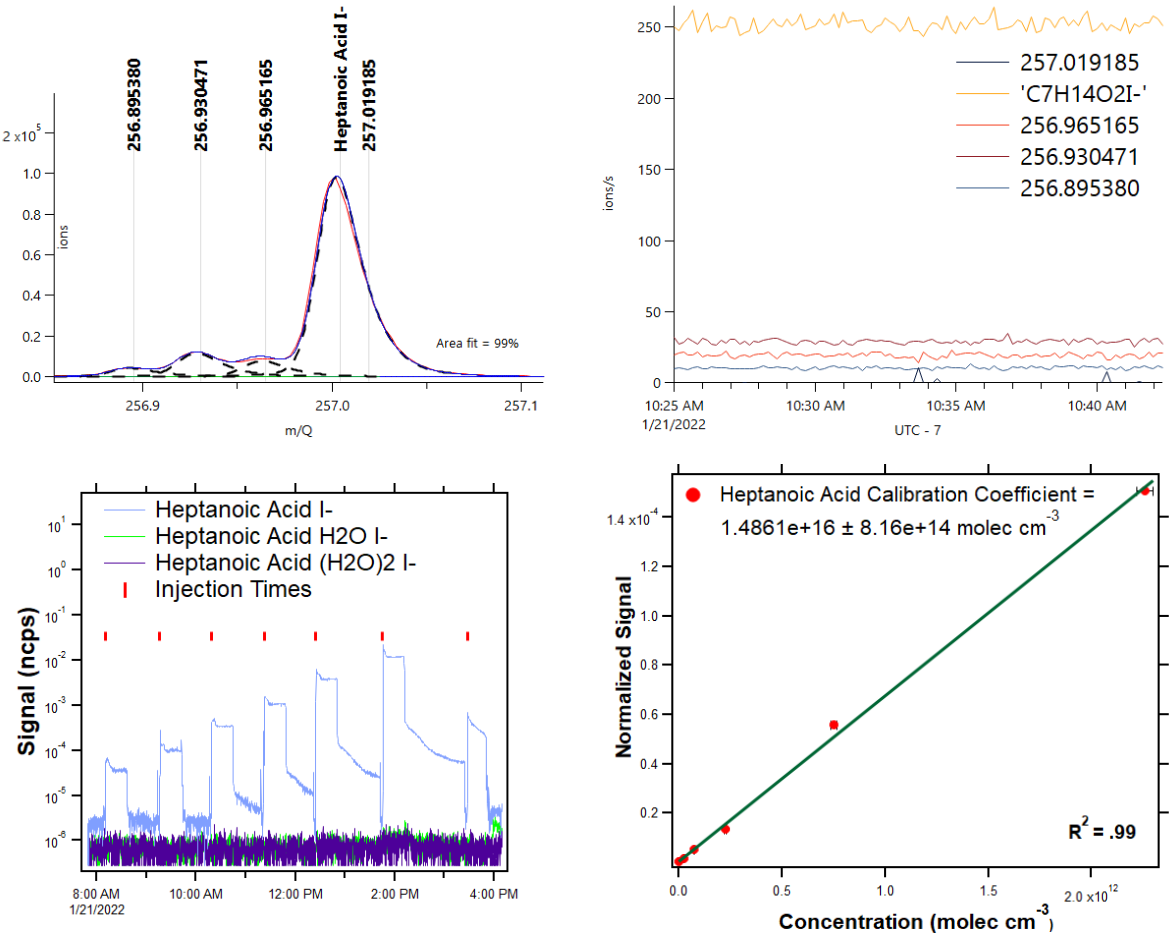

FIGURE 3.17: Characterization of heptanoic acid: The detected heptanoic acid I- peak shape at m/z=257 (top left), the time series of heptanoic acid I- (top right), heptanoic acid I- hydrates (bottom left), and the preliminary heptanoic acid calibration coefficient of 1.49E+16 +/- 8.16E+14 molecules/cm^3.

equation below.

$$[C_7H_{14}O_2] \;=\; 1.5\;x\;10^{16}\;molec.\,cm^{-3}\;x\;\frac{C_7H_{14}O_2\cdot I^-}{(I^- + H_2O\cdot I^- + C_2H_3N\cdot I^-)}\;-6.1\;x\;10^{-6} \tag{3.4}$$

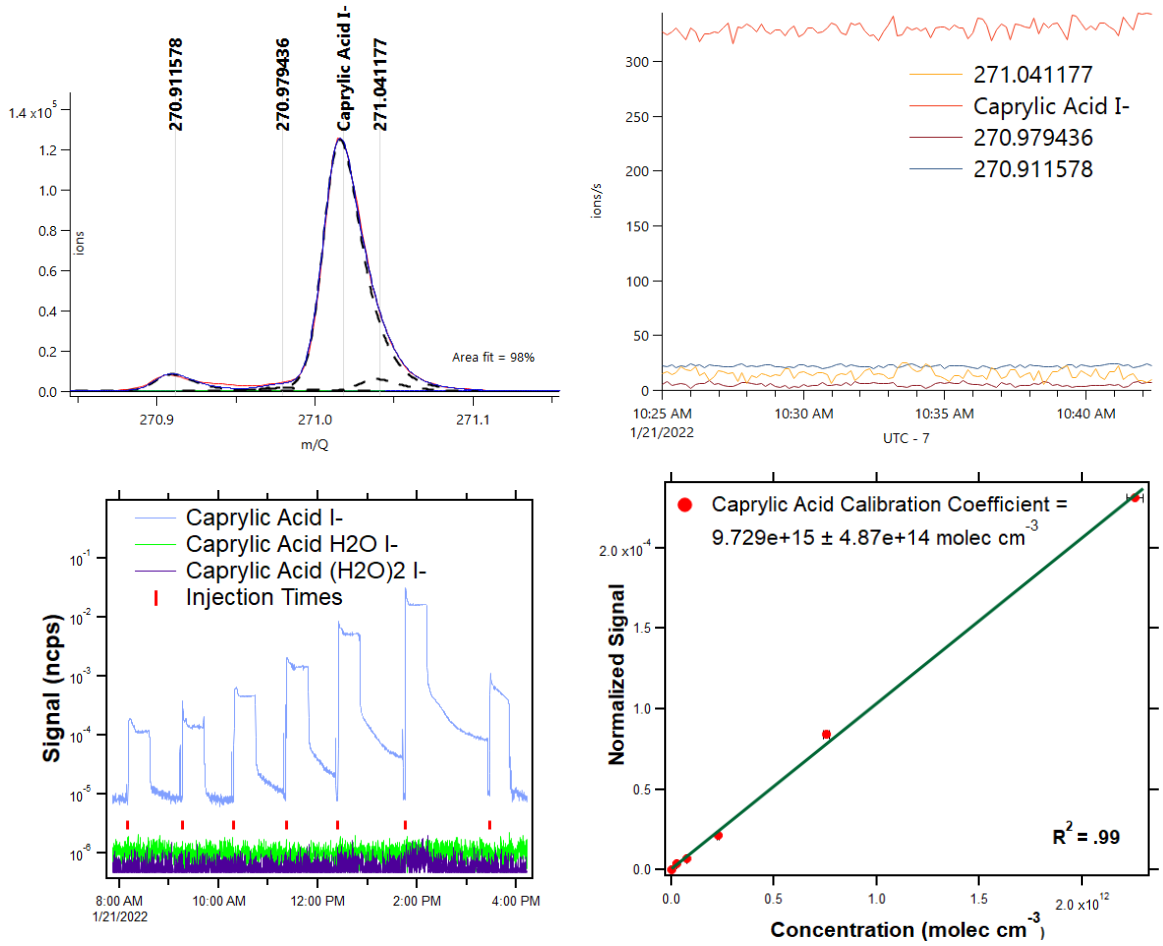

FIGURE 3.18: Characterization of caprylic acid: The detected caprylic acid I- peak shape at m/z=271 (top left), the time series of caprylic acid I- (top right), caprylic acid I- hydrates (bottom left), and the preliminary caprylic acid calibration coefficient of 9.73E+15 +/- 4.87E+14 molecules/cm^3.

3.4.5 The Characterization of Caprylic Acid

Caprylic acid or octanoic acid is a carboxylic acid with seven carbon atoms and a carboxyl group. The octanoic acid iodide cluster has a nominal mass of 271. There are five peaks present at the nominal mass of 271: caprylic acid I-, an unknown peak at 270.819884 amu, an unknown peak at 270.980686 amu, an unknown peak at 271.041710 amu, and an unknown peak at 270.911990 amu. The caprylic acid I- peak is present at

around 322 ions/s. The 270.819884 peak is present at 4 ions/s. The 270.980686 peak is present at 5 ions/s. The 271.041710 peak is present at 16 ions/s. The 270.911990 peak is present at 23 ions/s. The caprylic acid I- water cluster is present at negligible quantities. The calibration curve for caprylic acid is presented in Figure 3.18. As one of the "compounds that evaporate with their solvent", caprylic acid has a linear calibration coefficient of 9.73E+15 +/- 4.87E+14 molecules/cm^3 as displayed in the equation below.

$$[C_8H_{16}O_2] \;=\; 9.73\ x\ 10^{15}\ molec.\ cm^{-3}\ x\ \frac{C_8H_{16}O_2 \cdot I^-}{(I^- + H_2O \cdot I^- + C_2H_3N \cdot I^-)}\ - 1.0\ x\ 10^{-6} \tag{3.5}$$

3.4.6 The Characterization of Ethylene Glycol

Ethylene glycol is an alcohol with two carbon atoms and two alcohol groups. The ethylene glycol iodide cluster has a nominal mass of 189. There are two peaks present at the nominal mass of 189: ethylene glycol I- and an unknown peak at 188.920013 amu. The ethylene glycol I- peak is present at 650 ions/s. The 188.920013 peak is present at 4700 ions/s. The ethylene glycol I- water cluster is present at negligible quantities. The calibration curve for ethylene glycol is present above. While ethylene glycol is one of the "compounds that evaporate with their solvent", the periods of stability are more variable than the compounds that have been discussed previously. As such, the calibration curve as presented in Figure 3.19 is not perfectly linear as expected, and there is no preliminary calibration coefficient to report.

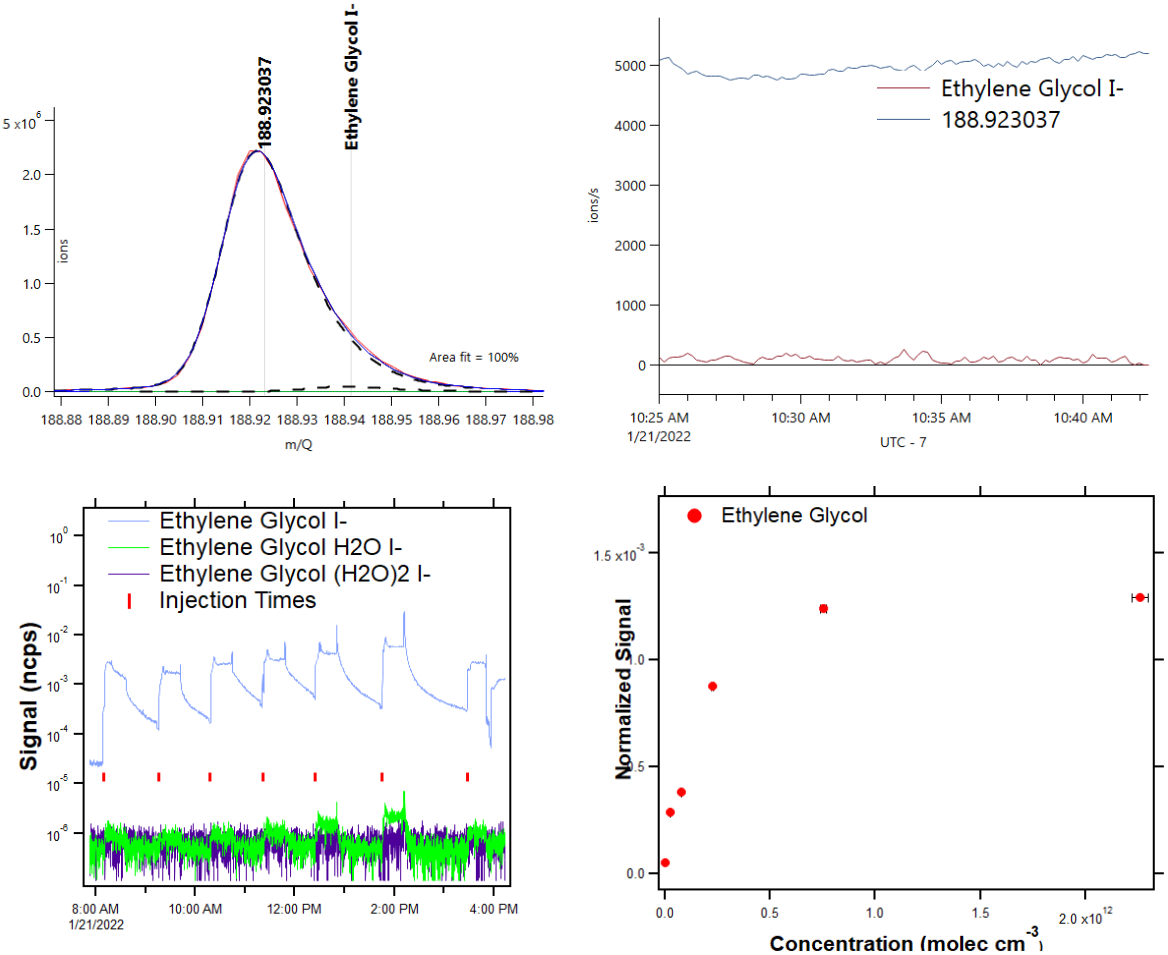

FIGURE 3.19: Characterization of ethylene glycol: The detected ethylene glycol I- peak shape at m/z=189 (top left), the time series of ethylene glycol I- (top right), ethylene glycol I- hydrates (bottom left), and there is not a preliminary calibration coefficient to report at this time

3.4.7 The Characterization of Glyoxylic Acid

Glyoxylic acid or oxoacetic acid is a carboxylic acid with a carbonyl group and a carboxyl group. The glyoxylic acid iodide cluster has a nominal mass of 201. Glyoxylic acid is the only peak present at the nominal mass of 201. The glyoxylic acid I- peak is present at 1400 ions/s. The glyoxylic acid I- water cluster is present at low quantities. The calibration curve for glyoxylic acid is presented in Figure 3.20. Glyoxylic acid is

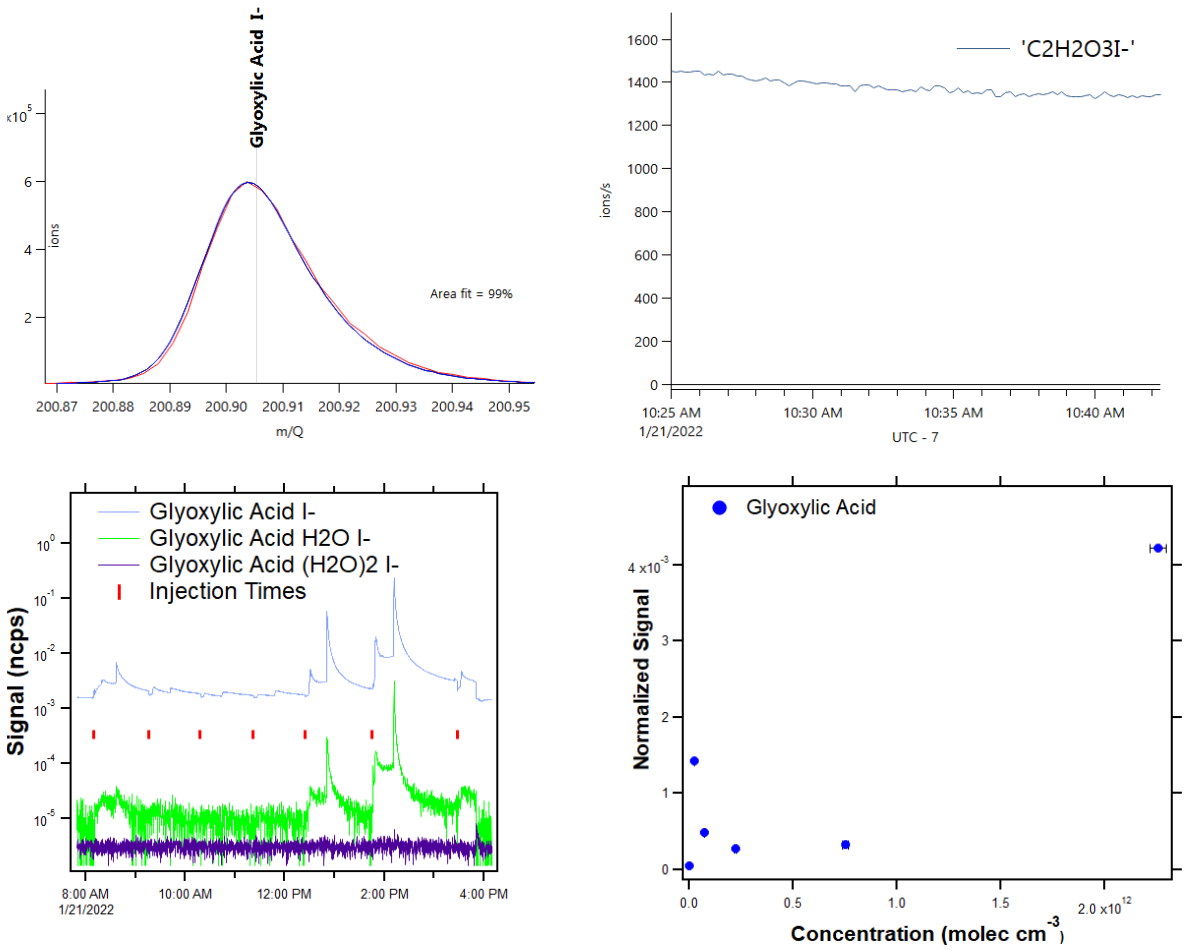

FIGURE 3.20: Characterization of glyoxylic acid: The detected glyoxylic acid I- peak shape at m/z=201 (top left), the time series of glyoxylic acid I- (top right), glyoxylic acid I- hydrates (bottom left), and the preliminary glyoxylic acid calibration curve. As glyoxylic acid is one of the "compounds that evaporate after their solvent", there is not a preliminary calibration coefficient to report at this time.

one of the "compounds that evaporate after their solvent", and a stable signal was never achieved. While the signal is observed to increase with the gas-phase concentration, the points do not fall on a linear calibration curve like those of the generally well-behaved acids. As such, there is no preliminary calibration coefficient to report.

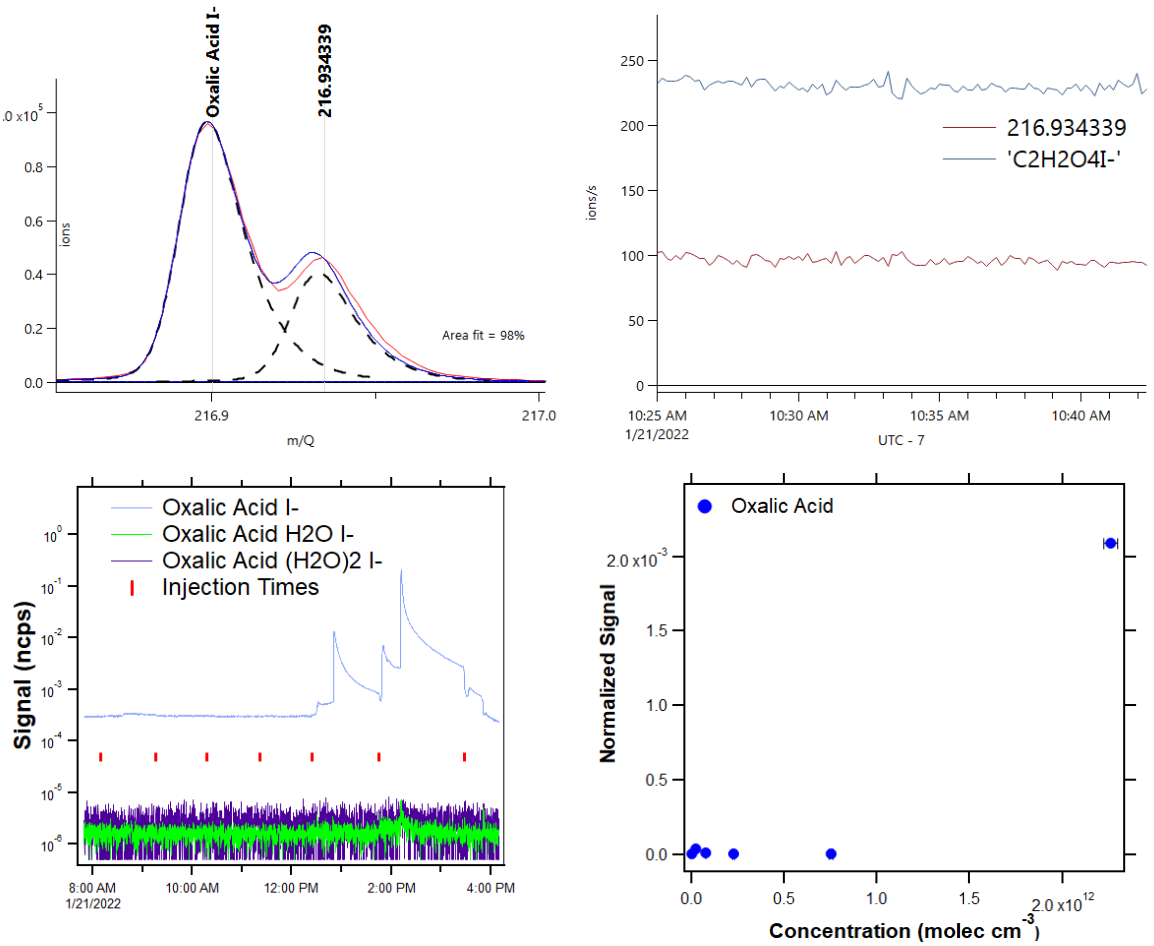

FIGURE 3.21: Characterization of oxalic acid: The detected oxalic acid I- peak shape at m/z=217 (top left), the time series of oxalic acid I- (top right), oxalic acid I- hydrates (bottom left), and the preliminary oxalic acid calibration curve. As oxalic acid is one of the "compounds that evaporate after their solvent", there is not a preliminary calibration coefficient to report at this time.

3.4.8 The Characterization of Oxalic Acid

Oxalic acid or ethanedioic acid is a dicarboxylic acid consisting of two carboxyl groups. The oxalic acid Iodide cluster has a nominal mass of 217. There are two peaks present at the nominal mass of 217: the oxalic acid I- peak and an unknown peak at a mass of 216.934339 amu. The oxalic acid I- peak is present at around 232 ions/s. The

216.934339 peak is present at around 100 ion/s. The oxalic acid I- water cluster is not present. The calibration curve for oxalic acid is presented in Figure 3.20. Oxalic acid is one of the "compounds that evaporate after their solvent", and a stable signal was never achieved. While the signal is observed to increase with the gas-phase concentration, the points do not fall on a linear calibration curve like those of the generally well-behaved acids. As such, there is no preliminary calibration coefficient to report.

3.4.9 The Characterization of Malonic Acid

Malonic acid or propanedioic acid is a dicarboxylic acid consisting of a carbon atom and two carboxyl groups. The malonic acid iodide cluster has a nominal mass of 231. There are four peaks present at the nominal mass of 231: The malonic acid I- peak, an unknown peak at 231.122453 amu, an unknown peak at 230.877076 amu, and an unknown peak at 230.948560 amu. The malonic acid I- peak is present at around 320 ions/s. The 231.122453 peak is present at 0.3 ions/s. The 230.877076 peak is present at 5 ions/s. The 230.948560 peak is present at 10 ions/s. The calibration curve for Malonic Acid is presented in Figure 3.22. Malonic Acid is one of the "compounds that evaporate after their solvent", and a stable signal was never achieved. While the signal is observed to increase with the gas-phase concentration, the points do not fall on a linear calibration curve like those of the generally well-behaved acids. As such, there is no preliminary calibration coefficient to report.

3.4.10 The Characterization of Succinic Acid

Succinic acid or butanedioic acid is a dicarboxylic acid with two carbon atoms and two carboxyl groups. The succinic acid iodide cluster has a nominal mass of 245. There are four peaks present at the nominal mass of 245: The succinic acid I- peak,

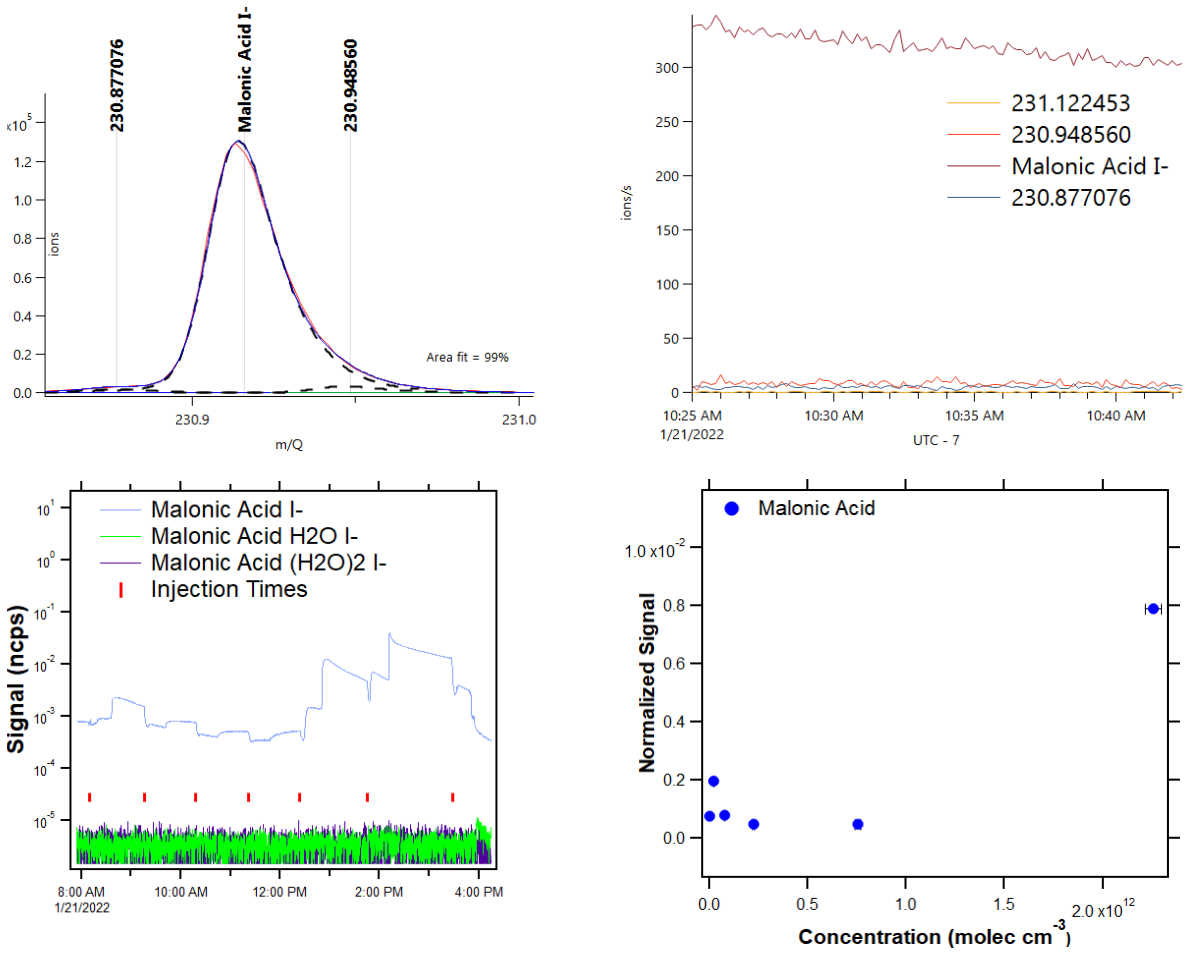

FIGURE 3.22: Characterization of malonic acid: The detected malonic acid I- peak shape at m/z=231 (top left), the time series of malonic acid I- (top right), malonic acid I- hydrates (bottom left), and the preliminary malonic acid calibration curve. As malonic acid is one of the "compounds that evaporate after their solvent", there is not a preliminary calibration coefficient to report at this time.

the 1,2-ISOPOOH I- peak at 244.961951 amu, an unknown peak at 244.990930 amu, and an unknown peak at 244.901235 amu. The succinic acid I- peak is present at 250 ions/s. The 1,2-ISOPOOH I- peak is present at 6 ions/s. The 244.990930 peak is present at 2 ions/s. The 244.901235 peak is present at 6 ions/s. The calibration curve for succinic acid is presented in Figure 3.23. Succinic acid is one of the "compounds that

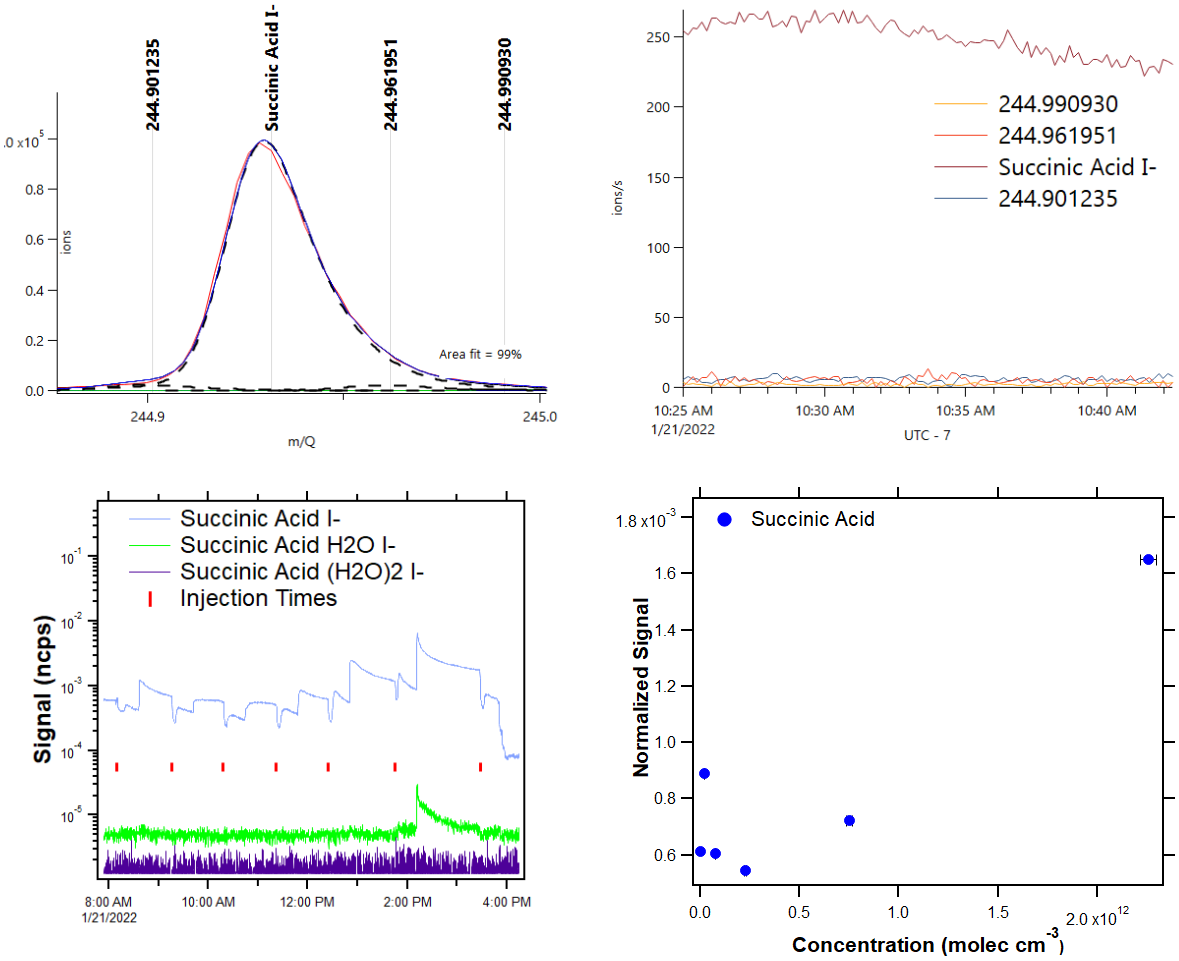

FIGURE 3.23: Characterization of succinic acid: The detected succinic acid I- peak shape at m/z=245 (top left), the time series of succinic acid I- (top right), succinic acid I- hydrates (bottom left), and the preliminary succinic acid calibration curve. As succinic acid is one of the "compounds that evaporate after their solvent", there is not a preliminary calibration coefficient to report at this time.

evaporate after their solvent", and a stable signal was never achieved. While the signal is observed to increase with the gas-phase concentration, the points do not fall on a linear calibration curve like those of the generally well-behaved acids. As such, there is no preliminary calibration coefficient to report.

3.4.11 Characterization Summary Table

Calibration Substance	Category	Calibration Coefficient (molecules/ cm^3)	Calibration Coefficient Uncertainty (molecules/ cm^3)	Calibration Coefficient *(cps/ppt) [normalized signal/ppt]	LOD (ppb)	Background Signal (normalized signal)	Multiple Peaks at Nominal Mass	O/C	Functional Groups Present	Structure
Formic Acid	Evaporates With Solvent	4.81E+13	1.01E+12	.360 [0.514]	9.9	4.95E-3	No	2	Carboxylic Acid	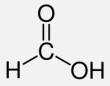
Acetic Acid	Evaporates With Solvent	7.48E+14	5.68E+12	.0221 [0.0331]	1.4	3.91E-5	No	1	Carboxylic Acid	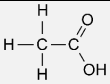
Hexanoic Acid	Evaporates With Solvent	2.15E+16	4.74E+14	.0637 [0.0947]	.099	2.46E-6	Yes	.33	Carboxylic Acid	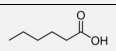
Heptanoic Acid	Evaporates With Solvent	1.49E+16	8.16E+14	.0887 [0.132]	.048	2.39E-6	Yes	.28	Carboxylic Acid	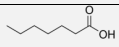
Caprylic Acid	Evaporates With Solvent	9.73E+15	4.87E+14	.123 [0.181]	.060	8.38E-6	Yes	.25	Carboxylic Acid	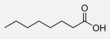
Ethylene Glycol	Evaporates With Solvent	----------	----------	----------	-------	2.65E-5	Yes	1	Alcohol	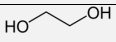
Glyoxylic Acid	Evaporates After Solvent	----------	----------	----------	-------	1.60E-3	No	1.7	Carboxylic Acid and Aldehyde	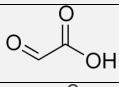
Oxalic Acid	Evaporates After Solvent	----------	----------	----------	-------	2.94E-4	Yes	2	Carboxylic Acids	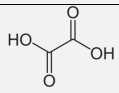
Malonic Acid	Evaporates After Solvent	----------	----------	----------	-------	8.05E-4	Yes	1.3	Carboxylic Acids	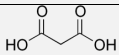
Succinic Acid	Evaporates After Solvent	----------	----------	----------	-------	6.12E-4	Yes	1	Carboxylic Acids	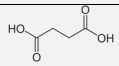

*** Parent Ion Signal: I- signal = 1.6E+5 cps, H_2O I- = 1.4E+5 cps, Acetonitrile I- = 2.2E+4 cps**

TABLE 3.5: A characterization summary table of all calibration compounds measured during preliminary calibration testing on the LTOF CIMS. The unit in the table as expressed as molecules/cm^3 is related to the community standard of cps/ppt in the following manner: The number of air molecules in 1 cm^3 is divided by the number of calibration substance molecules in 1 cm^3. This is the inverse of the volume mixing ratio. When multiplied by 10^{-12}, this number is expressed as ppt^{-1}. The signal detected by the CIMS in cps is then multipled by the inverse volume mixing ratio to arrive at cps/ppt. The unit of normalized signal (cps cps^{-1}) per ppt refers to the detected signal normalized to the parent ion signals, denoted by the * under the table.

3.5 Binding Enthalpy and O/C Ratio

3.5.1 Sensitivity vs Binding Enthalpy

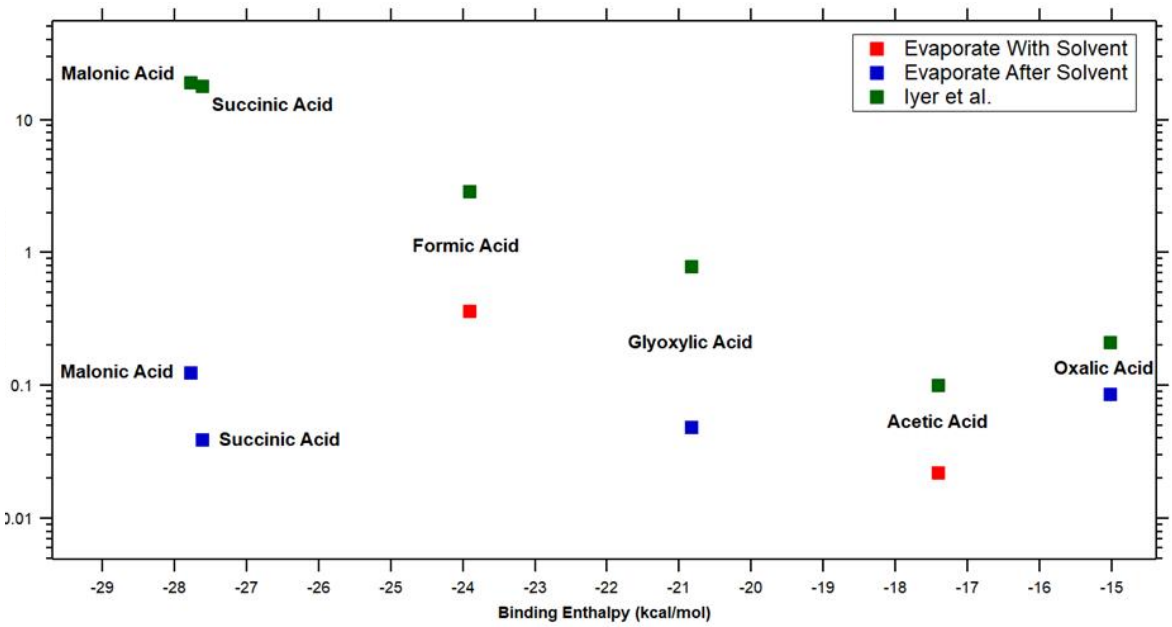

FIGURE 3.24: Sensitivity in cps/ppt vs the Binding Enthalpy in kcal/mol [35] for the compounds that were measured in this study and in Iyer et al. The sensitivities measured in this study are lower than those reported in Iyer et al. However, the measurements follow the same general shape. The sensitivities plotted for the "compounds that evaporate after their solvent" are approximated based on the general shape of the calibration curves.

Figure 2.24 is a plot of sensitivity in cps/ppt vs binding enthalpy in kcal/mol. The binding enthalpies for the compounds included in the plot are reported in Iyer et al. The red squares are the "compounds that evaporate with their solvent". The blue squares are the "compounds that evaporate after their solvent". The green squares are the values reported in Iyer et al. Not all of the calibration compounds measured are displayed on this figure; only compounds that were also measured and reported by Iyer et al. are displayed for comparison. The sensitivity measurements for this study are lower than those made by Iyer et al. However, with the exception of malonic and

succinic acids, the compounds have the same general shape. It is worth noting that the sensitivities plotted for the “compounds that evaporate after their solvent” are approximated from the non-linear calibration curves presented above. The sensitivities for Malonic and Succinic Acid are significantly lower than the values reported in literature. As can be seen in the time series above, the first few experimental runs for these acids drop below the background signal. The signals for the first few experimental runs also do not increase as the concentration increases. Because of this, the calibration curves observed for the “compounds that evaporate after their solvent" are lower than anticipated.

3.5.2 Oxygen/Carbon Ratio

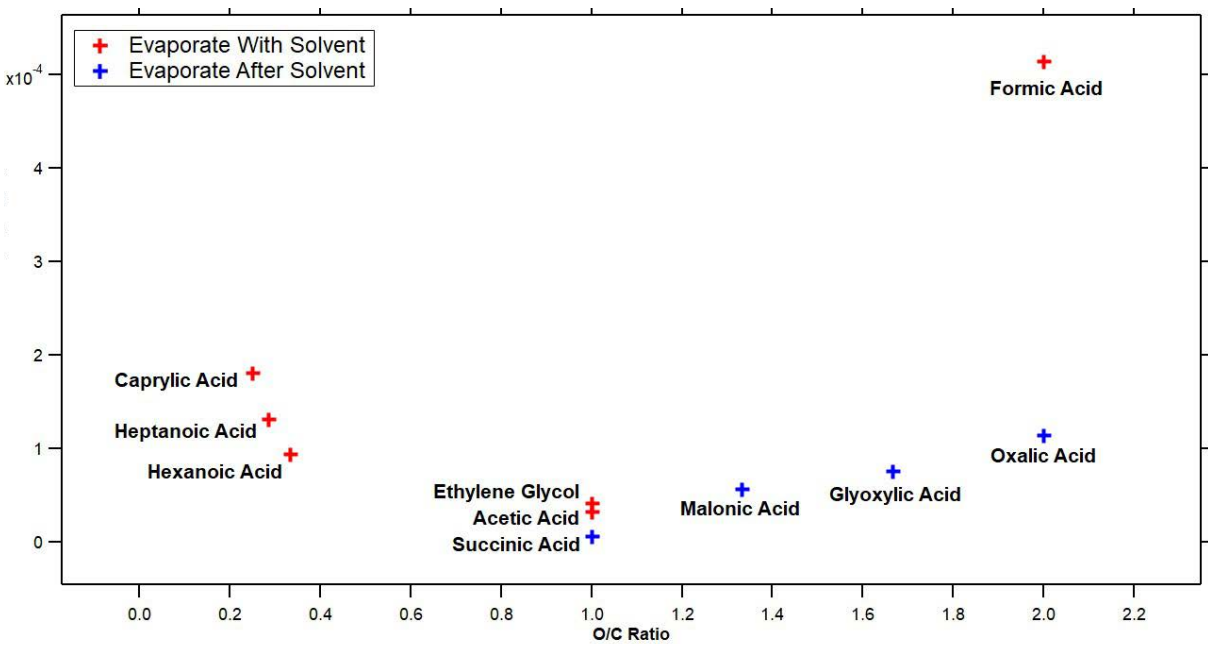

FIGURE 3.25: The measured calibration coefficients vs the oxygen to carbon (O/C) ratio for each calibration compound. The “compounds that evaporate with their solvent” are noted by red crosses and the “compounds that evaporate after their solvent” are noted by blue crosses.

Figure 2.25 is a plot of calibration coefficients in ncps/ppb vs the oxygen to carbon (O/C) ratio for each calibration coefficient. The calibration coefficients for the "compounds that evaporate after their solvent" are approximated from the calibration curves presented in section 3.4. As these calibration coefficients are approximations from non-linear curves, they will not be reported independently as preliminary calibration coefficients. With the exception of formic acid, "compounds that evaporate with their solvent" follow the same trend and the "compounds that evaporate after their solvent" follow the same trend. It appears that the calibration coefficients for the "compounds that evaporate with their solvent" (red) decrease as the O/C ratio increases or as the carbon chain of the acid decreases. The calibration coefficients for the "compounds that evaporate after their solvent" appear to increase as the O/C ratio increases. One would expect the sensitivity (or calibration coefficient) of a compound to increase as the O/C ratio increases as oxygen participates in the cluster formation with iodide.

3.6 Background Characterization

3.6.1 Background Signal Comparison

After analyzing the calibration measurements made in January, consistently high backgrounds for some of the calibration coefficients have been identified. Furthermore, it was discovered that the acetonitrile flow was measured at 10 sccm as opposed to the set value of 30 sccm during calibration measurements. Because of this, the acetonitrile I- peak is lower than the H_2O I- peak, allowing for iodide water clusters to form, which in turn lowers the sensitivity of the compound iodide clusters and depletes the reagent ion. Figure 3.26 displays background signals for the calibration compounds at three different instrument states. On December 15th, 2021, 1,2-ISOPOOH was being

measured for the determination of a Henry's Law coefficient. At this point, none of the calibration compounds had been externally introduced to the CIMS. On December 17th, 2021, an initial calibration test with two of the compounds, ethylene glycol and caprylic acid, was measured with the CIMS in addition to 1,2-ISOPOOH. On January 21st, 2022, every calibration compound had been measured at various concentrations over the course of a three-week period. Comparing the signals measured on the 15th and the 17th, it is apparent that the background signals are greater on the 17th for almost all of the compounds, even though only two of the compounds had been formally introduced to the instrument. After analyzing further, it appears that the same acetonitrile set point issue was present at this time as well, meaning that the acetonitrile was not present in a high enough concentration to prevent the formation of water clusters. Comparing the 17th of December with the 21st of January, it is also apparent that the background signals are greater on the 21st for almost all of the compounds. Both the 17th and the 21st had lower acetonitrile concentrations than anticipated, so the only difference between the two days is the introduction of the calibration compounds. This allows some insight into the stickiness of the lines and the state of the instrument following weeks of calibration runs.

3.6.2 Moving Forward

The two categories of compounds, those that evaporate with their solvent and those that evaporate after their solvent, will be measured in different solutions in the future to allow for better switching times. Additionally, the two categories of compounds will be measured with different solvents: the "compounds that evaporate after their solvents" will be tested with solvents that are less polar than water such as to see if 1) this provides better stability and 2) this brings the background signal down. Finally, the

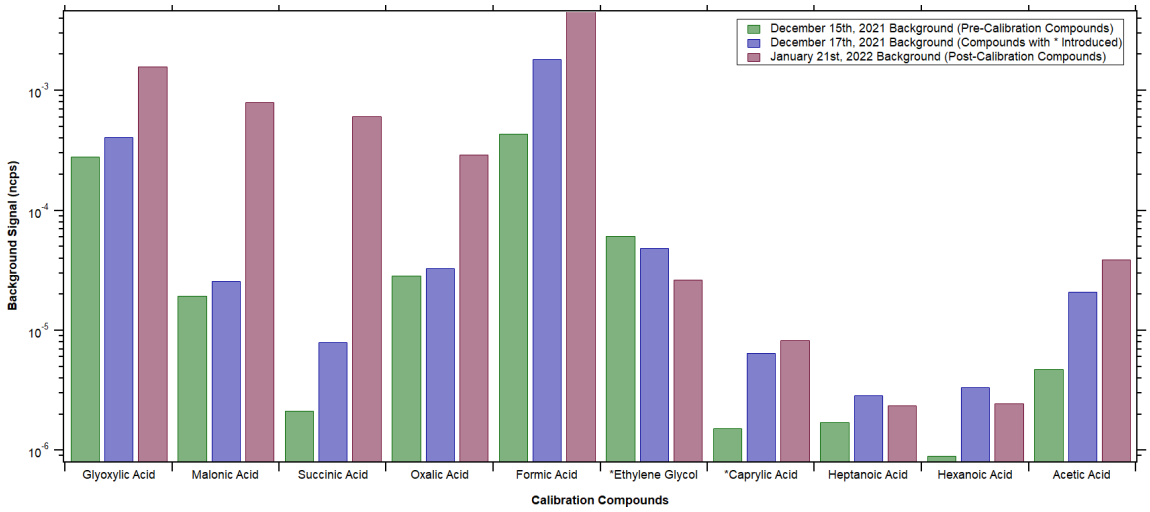

FIGURE 3.26: Calibration compound background signals (ncps) measured with the LTOF-CIMS on December 15th, 2021 (green, first), December 17th, 2021 (purple, second), and January 21st, 2022 (red, third). On December 15th, only 1,2-ISOPOOH was injected into the CIMS. On December 17th, 1,2-ISOPOOH, ethylene glycol, and caprylic acid were injected into the CIMS. On January 21st, all calibration compounds had been injected into the CIMS.

presence of acetonitrile in higher concentrations will prevent significant water clustering in future runs, allowing for better sensitivity, lower background, and less reagent ion depletion.

4 Conclusion

Two methods were developed and tested to quantify gas-phase signals detected with a VOCUS 2R API-LToF mass spectrometer. The integration method was applied to 1,2-ISOPOOH partitioning experiments to determine the Henry's Law coefficient, which was determined to be 2.61E+05 M/atm +/- 1.81E+04 M/atm. The flow rate method was applied during initial calibration development to determine preliminary calibration coefficients for a suite of selected oxygenated hydrocarbons (mono- di-, and multifuncational carboxylic acids, dicarbonyls, alcohols) in preparation for the TI^{3}GER campaign. After initial calibration testing, two groups of compounds emerged: those that evaporate with their solvent and those that evaporate after their solvent. The compounds that evaporate after their solvent consist solely of dicarbonyls. Stable signal is observed for the compounds that evaporate with their solvent while a decaying signal is observed for those that do not evaporate with their solvent. For optimal measurements, compounds should be measured separately, depending on the evaporation rate of their solvent. The partitioning and syringe pump setups can be used in future work to determine Henry's Law coefficients and Setschenow salting coefficients. The flow rate method will continue to be optimized for future laboratory and aircraft calibrations.

Bibliography

(1) Sharkey, T. D.; Wiberley, A. E.; Donohue, A. R. *Annals of Botany* **2007**, *101*, 5–18.

(2) Guenther, A.; Karl, T.; Harley, P.; Wiedinmyer, C.; Palmer, P. I.; Geron, C. *Atmospheric Chemistry and Physics* **2006**, *6*, 3181–3210.

(3) Saiz-Lopez, A.; Plane, J. M. C.; Baker, A. R.; Carpenter, L. J.; von Glasow, R.; Gómez Martín, J. C.; McFiggans, G.; Saunders, R. W. *Chemical Reviews* **2012**, *112*, PMID: 22032347, 1773–1804.

(4) Shrivastava, M. et al. *Reviews of Geophysics* **2017**, *55*, 509–559.

(5) Kampf, C. J.; Waxman, E. M.; Slowik, J. G.; Dommen, J.; Pfaffenberger, L.; Praplan, A. P.; Prévôt, A. S. H.; Baltensperger, U.; Hoffmann, T.; Volkamer, R. *Environmental Science & Technology* **2013**, *47*, PMID: 23534917, 4236–4244.

(6) Waxman, E. M.; Elm, J.; Kurtén, T.; Mikkelsen, K. V.; Ziemann, P. J.; Volkamer, R. *Environmental Science & Technology* **2015**, *49*, PMID: 26335375, 11500–11508.

(7) Kurtén, T.; Elm, J.; Prisle, N. L.; Mikkelsen, K. V.; Kampf, C. J.; Waxman, E. M.; Volkamer, R. *The Journal of Physical Chemistry A* **2015**, *119*, PMID: 25408201, 4509–4514.

(8) Sareen, N.; Waxman, E. M.; Turpin, B. J.; Volkamer, R.; Carlton, A. G. *Environmental Science & Technology* **2017**, *51*, PMID: 28169540, 3327–3335.

(9) Sander, R. *Atmospheric Chemistry and Physics* **2015**, *15*, 4399–4981.

(10) Endo, S.; Pfennigsdorff, A.; Goss, K.-U. *Environmental Science & Technology* **2012**, *46*, PMID: 22191628, 1496–1503.

(11) Waxman, E. M.; Elm, J.; Kurtén, T.; Mikkelsen, K. V.; Ziemann, P. J.; Volkamer, R. *Environmental Science & Technology* **2015**, *49*, PMID: 26335375, 11500–11508.

(12) Ruckenstein, E.; Shulgin, I. *Industrial & Engineering Chemistry Research* **2002**, *41*, 4674–4680.

(13) Toivola, M.; Prisle, N. L.; Elm, J.; Waxman, E. M.; Volkamer, R.; Kurtén, T. *The Journal of Physical Chemistry A* **2017**, *121*, PMID: 28758400, 6288–6295.

(14) Koenig, T. K.; Volkamer, R.; Apel, E. C.; Bresch, J. F.; Cuevas, C. A.; Dix, B.; Eloranta, E. W.; Fernandez, R. P.; Hall, S. R.; Hornbrook, R. S.; Pierce, R. B.; Reeves, J. M.; Saiz-Lopez, A.; Ullmann, K. *Science advances* **2021**, *7*, eabj6544.

(15) McFiggans, G.; Coe, H.; Burgess, R.; Allan, J.; Cubison, M.; Alfarra, M. R.; Saunders, R.; Saiz-Lopez, A.; Plane, J. M. C.; Wevill, D.; Carpenter, L.; Rickard, A. R.; Monks, P. S. *Atmospheric Chemistry and Physics* **2004**, *4*, 701–713.

(16) Wang, M. et al. *Atmospheric Measurement Techniques* **2021**, *14*, 4187–4202.

(17) Koenig, T. K.; Baidar, S.; Campuzano-Jost, P.; Cuevas, C. A.; Dix, B.; Fernandez, R. P.; Guo, H.; Hall, S. R.; Kinnison, D.; Nault, B. A.; Ullmann, K.; Jimenez, J. L.; Saiz-Lopez, A.; Volkamer, R. *Proceedings of the National Academy of Sciences* **2020**, *117*, 1860–1866.

(18) Wang, M. et al. *Atmospheric Measurement Techniques* **2021**, *14*, 4187–4202.

(19) Vocus CI-TOF - online detection of vocs, 2022.

(20) Lee, B. H.; Lopez-Hilfiker, F. D.; Mohr, C.; Kurtén, T.; Worsnop, D. R.; Thornton, J. A. *Environmental Science & Technology* **2014**, *48*, PMID: 24800638, 6309–6317.

(21) Deming, B. L.; Pagonis, D.; Liu, X.; Day, D. A.; Talukdar, R.; Krechmer, J. E.; de Gouw, J. A.; Jimenez, J. L.; Ziemann, P. J. *Atmospheric Measurement Techniques* **2019**, *12*, 3453–3461.

(22) Pagonis, D.; Krechmer, J. E.; de Gouw, J.; Jimenez, J. L.; Ziemann, P. J. *Atmospheric Measurement Techniques* **2017**, *10*, 4687–4696.

(23) https://webbook.nist.gov/cgi/cbook.cgi?ID=C78795&Units=SI&Mask=1F#ref-16).

(24) Daubert, T. E. (E. Physical and thermodynamic properties of pure chemicals : data compilation.

(25) https://webbook.nist.gov/cgi/cbook.cgi?ID=C64186&Mask=4#ref-14).

(26) https://webbook.nist.gov/cgi/cbook.cgi?ID=C64197&Mask=4#ref-16).

(27) https://webbook.nist.gov/cgi/cbook.cgi?ID=C142621&Units=SI&Mask=F#ref-15).

(28) https://webbook.nist.gov/cgi/cbook.cgi?ID=C111148&Mask=4#ref-10).

(29) https://webbook.nist.gov/cgi/cbook.cgi?ID=C124072&Mask=4#ref-12).

(30) https://webbook.nist.gov/cgi/cbook.cgi?ID=C107211&Mask=4#ref-16).

(31) https://webbook.nist.gov/cgi/cbook.cgi?ID=C64197&Mask=4#ref-16).

(32) Bilde, M.; Svenningsson, B.; Mønster, J.; Rosenørn, T. *Environmental Science & Technology* **2003**, *37*, 1371–1378.

(33) https://webbook.nist.gov/cgi/cbook.cgi?ID=C108305&Mask=E#ref-9).

(34) Ranney, A. P.; Ziemann, P. J. *Aerosol Science and Technology* **2016**, *50*, 881–892.

(35) Iyer, S.; Lopez-Hilfiker, F.; Lee, B. H.; Thornton, J. A.; Kurtén, T. *The Journal of Physical Chemistry A* **2016**, *120*, PMID: 26736021, 576–587.

5 Appendix

5.1 Syringe Pump Experimental Procedure

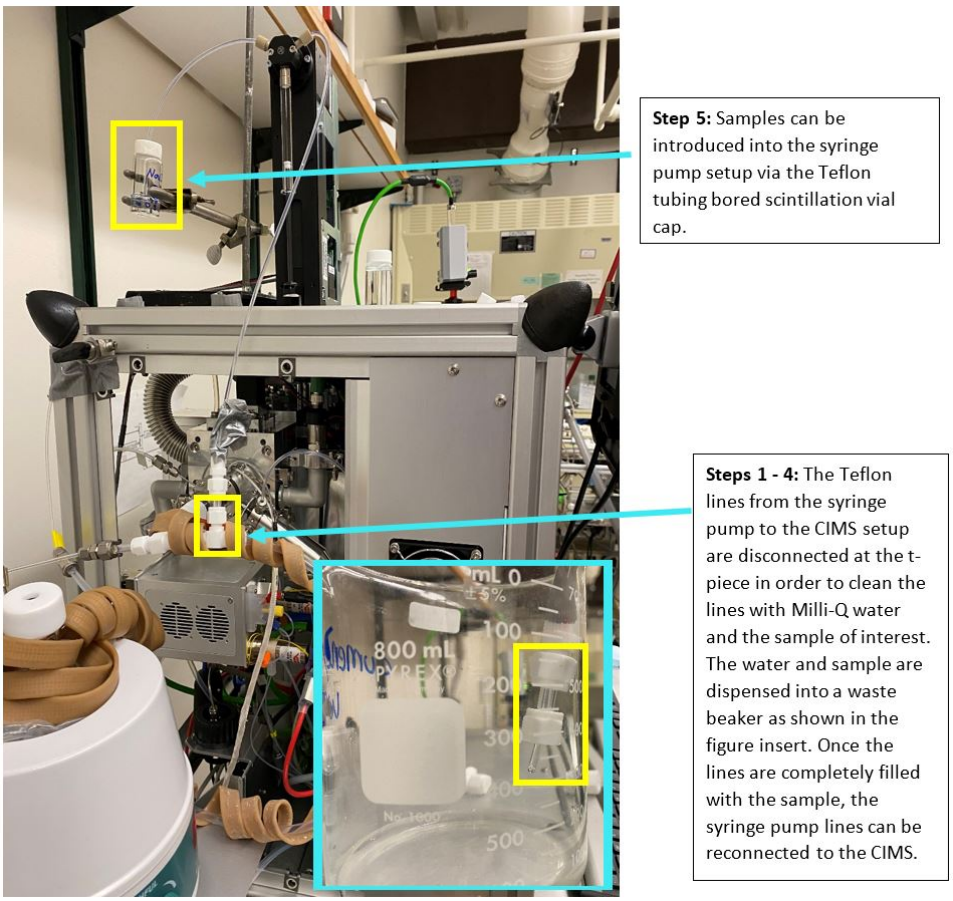

1) Check to ensure proper parameters are in place (i.e. syringe, line heating, dilution flow).The following figure provides the flow rate range in uL/min, the volume of the syringe, the set speed and the actual speed in steps/second, the injection time in minutes, and the flow rate in uL/min. The actual speed is the number of steps (the syringe pump defines the entire volume of a syringe to be 6000 steps) the syringe pump will move per second. Upon initial testing and observation, it was discovered that the speed command issued to the syringe pump must be twice the actual speed

desired. Thus, the set speed is the command issued to the syringe pump in order to achieve the "actual" or desired speed. The line heating and dilution flow parameters are described above in section xyz of this thesis.

Flow Rate Range (uL/min)	Volume (uL)	Stroke Length (Steps)	Set Vx (Steps/second)	Actual Vx (steps/second)	Time (min)	Flow Rate
Min (1)	100	6000	2	1	100	1
5	100	6000	10	5	20	5
7.5	100	6000	15	7.5	13	7.5
10	100	6000	20	10	10	10
12.5	100	6000	25	12.5	8	12.5
15	100	6000	30	15	7	15
Max (5000)	100	6000	10000	5000	0	5000
Flow Rate Range (uL/min)	Volume (uL)	Stroke Length (Steps)	Set Vx (Steps/second)	Actual Vx (steps/second)	Time (min)	Flow Rate
Min (2.5)	250	6000	2	1	100	2.5
5	250	6000	4	2	50	5
7.5	250	6000	6	3	33	7.5
10	250	6000	8	4	25	10
12.5	250	6000	10	5	20	12.5
15	250	6000	12	6	17	15
Max (12500)	250	6000	10000	5000	0	12500
Flow Rate Range (uL/min)	Volume (uL)	Stroke Length (Steps)	Set Vx (Steps/second)	Actual Vx (steps/second)	Time (min)	Flow Rate
Min (5)	500	6000	2	1	100	5
5	500	6000	2	1	100	5
7.5	500	6000	3	1.5	67	7.5
10	500	6000	4	2	50	10
12.5	500	6000	5	2.5	40	12.5
15	500	6000	6	3	33	15
Max (25000)	500	6000	10000	5000	0	25000
Flow Rate Range (uL/min)	Volume (uL)	Stroke Length (Steps)	Set Vx (Steps/second)	Actual Vx (steps/second)	Time (min)	Flow Rate
Min (10)	1000	6000	2	1	100	10
5	1000	1500	2	1	25	10
7.5	1000	6000	-	-	-	-
10	1000	6000	2	1	100	10
12.5	1000	6000	-	-	-	-
15	1000	6000	3	1.5	67	15
Max (50000)	1000	6000	10000	5000	0	50000

2) Clean lines with Milli-Q water and dispense into waste beaker (as displayed above)

Command: /1gS7IA6000S7OA0G10R

***NOTE: The code will repeat this step 10 times

3) Fill lines completely with sample and dispense into waster beaker

Command: /1gS7IA6000S7OA0G10R

***NOTE: The code will repeat this step 10 times

4) Lines are reconnected to CIMS

***NOTE: Ensure that teflon tube goes into the glass wool placed inside the t-piece

5) Prepare to run the sample (xxxx steps, Vx = y)

Command: /1S7IAxxxxVyOA0R

Parameters for optimal signal:

Syringe: 250 uL

Flow Rate: 10.0 uL/min

Vx = 8

Line Heating = 15%

Dilution Flow = 2 slpm

Command:/1S7IA6000V8OA0R

6) Lines are disconnected from CIMS and sample line is removed from sample

7) Changing Samples or End of measurement day

If you are changing samples, connect the next sample to the setup via the teflon tubing

bored cap and follow step 3

***NOTE: Samples should increase in concentration.

If you are switching back to water, follow step 2 to clean the lines with water.

***NOTE: Refill the scintillation vial with fresh milli-Q water and repeat step 2 for a second time.